



The effect of Si/Al ratio of zeolite supported Pd for complete CH₄ oxidation in the presence of water vapor and SO₂

Ida Friberg, Nadezda Sadokhina, Louise Olsson*

Chemical Engineering, Competence Centre for Catalysis, Chalmers University of Technology, SE-412 96 Gothenburg, Sweden



ARTICLE INFO

Keywords:

Methane oxidation
Pd/beta
Pd/SSZ-13
SAR ratio
Sulfur poisoning and regeneration

ABSTRACT

The catalytic properties of palladium supported on H-beta and H-SSZ-13 zeolite with different silica to alumina ratio (SAR) have been evaluated for complete CH₄ oxidation in the presence and absence of water vapor and together with SO₂. Different SAR was successfully obtained by dealumination of the zeolites in an acidic solution at elevated temperature. Flow reactor experiments showed that the SAR of the zeolite support greatly impacts the catalytic activity, especially in the presence of water vapor. Pd supported on a highly siliceous beta zeolite expressed high and stable CH₄ conversion in the presence of water vapor, whereas the activity for Pd supported on zeolites with low SAR or Al₂O₃ decreased over time due to accumulative water deactivation. Hence, an increased SAR of the zeolite support clearly correlates to a lower degree of water deactivation. We suggest that this is a result of the high hydrophobicity of the siliceous zeolites. The results also imply that the catalytic activity in the presence of water vapor is influenced more by the SAR than the type of the zeolite framework. The CH₄ oxidation activity was also enhanced with increasing SAR under dry conditions. This was addressed to the formation of more Pd particles in relation to ion-exchanged Pd²⁺ species and changes of the oxidation-reduction behavior of the Pd. The high number of acidic sites in zeolites with low SAR provided higher dispersion of Pd particles and formation of more monoatomic Pd²⁺ species, whereas almost exclusively Pd particles of larger sizes were formed on the highly siliceous zeolites. The monoatomic Pd²⁺ species, mostly formed on zeolites with low SAR, were oxidized and reduced at significantly higher temperatures than Pd in the particle form. Hence, complete reduction or oxidation of the Pd supported on highly siliceous zeolites can be achieved at lower temperatures. Moreover, compared to Pd/Al₂O₃, the zeolite supported Pd expressed higher sensitivity to SO₂. However, the major part of the catalytic activity could be regenerated more easily using siliceous zeolites as supports compared to Al₂O₃. We suggest that this is an effect of the lower SO₂ adsorption on the zeolite supports than on the Al₂O₃ support, which results in the formation of more PdSO_x species upon SO₂ exposure. On the other hand, the low SO₂ adsorption on the zeolites also results in less spillover of sulfur species from the support to the active PdO, which explains the facilitated regeneration.

1. Introduction

Catalytic converters serve as important tools to abate environmental pollution arisen from combustion processes. One example is catalytic systems for complete oxidation of methane that remains in the exhaust gas due to incomplete combustion of for instance natural gas or biogas. The desire to completely oxidize the CH₄ residuals emanates from the fact that the oxidation product, CO₂, gives a significantly lower contribution to the greenhouse effect and the global warming than the corresponding amount of CH₄. Supported palladium catalysts are highly active for CH₄ oxidation and have therefore been the target for numerous research studies during the last decades. It has been found that

the active phase for CH₄ oxidation at moderate temperatures is oxidized Pd (PdO) [1], although many authors have reported that coexistence of PdO with metallic Pd is required for high activity [2–4]. However, at higher temperature ranges, metallic Pd tends to be the catalytically active phase [5].

It is well-known that the CH₄ oxidation activity is significantly reduced in the presence of water vapor [6] and SO₂ [7] on precious metal-based materials. Formation of hydroxyl species on the catalyst surface is responsible for the water deactivation. It is suggested that the surface hydroxyls block active PdO sites [8] and that the surface hydroxyls decrease oxygen exchange between support and Pd and thus limit the reoxidation of the Pd [9,10]. Furthermore, two categories of hydroxyls

* Corresponding author.

E-mail address: louise.olsson@chalmers.se (L. Olsson).

species have been distinguished; rapidly formed hydroxyls that causes immediate deactivation together with slowly formed hydroxyls with higher energy barrier which results in accumulative deactivation over time [11].

Exhaust gases generated from combustion of CH₄ based fuels typically have a very small content of sulfur compounds. However, SO₂ concentrations even below 1 ppm can result in significant deactivation of Pd based catalysts [12] and increased SO₂ concentrations have been reported to only influence the rate and not the degree of deactivation at steady-state conditions [13]. Furthermore, the deactivation mechanisms of Pd based catalyst have been suggested to be similar both upon the exposure to SO₂ and H₂S, since H₂S easily converts to form SO₂ under lean conditions [14,15]. Several authors have addressed the main reason for the deactivation to the formation of surface sulfates [7,13–17]. The coexistence of water vapor and SO₂ in the gas feed has been reported to accelerate the deactivation process of Pd/Al₂O₃ [7,18], since the water adsorption on the Al₂O₃ increases the sulfur spillover from the support to the PdO and/or decreases the sulfur spillover from the PdO to the support which results in the formation of more PdSO₄.

The CH₄ oxidation activity as well as the resistance against water and sulfur deactivation of Pd based catalysts are greatly influenced by the choice of support material. Thus, support modification is one strategy to mitigate the problems with water and sulfur deactivation. This can be done either by using completely different support materials, in terms of composition and structure, or by addition of different promoters. Aluminosilicate zeolites are one promising group of alternative support which has been investigated in several studies [19–22]. Okumura et al. [21] found that the CH₄ oxidation activity over Pd supported on zeolite H-beta and H-ZSM-5 is highly dependent upon the silica to alumina (SAR) ratio of the zeolite framework. They showed that an increased SAR (up to Si/Al₂ = 1100) correlates to a higher CH₄ oxidation activity, both under dry and wet conditions. By contrast, Pd/SiO₂ typically has lower activity in comparison to both Pd upon siliceous zeolites [21] and Pd/Al₂O₃ [23,24]. This fact indicates that not only the Si content but also the zeolite structure play a crucial role on the catalytic activity. The high activity and the resistance against water deactivation of Pd supported on siliceous zeolites may be attributed to the formation of highly active PdO agglomerates due to the low number of stabilizing acidic sites in the zeolite framework [21] and to the high hydrophobicity of zeolites with a high silica content resulting in less water adsorption [21,25]. Moreover, Lim et al. [19] recently showed that Pd/SSZ-13 (Si/Al = 16) gives significantly higher and more stable CH₄ conversion in the presence of water vapor compared to Pd/Al₂O₃ and Pd supported on other small pore zeolites. However, this effect was ascribed to less Pd sintering and dealumination due to the high acidity of the SSZ-13 zeolite. Furthermore, the acidity of the zeolite support can also be altered by exchanging the protons on the acidic zeolite sites with sodium cations [22]. Petrov et al. [22] recently showed that the water vapor induced Pd sintering was significantly suppressed on fully sodium exchange Pd/Na-MOR zeolite, resulting in high and stable CH₄ oxidation activity in the presence of water vapor.

The support materials also have a crucial impact on the sulfur tolerance of the catalyst. It has for instance been shown that Pd on non-sulfating supports, such as SiO₂, becomes more rapidly deactivated compared to Pd on sulfating supports like Al₂O₃ [12,16,24]. The suggested explanation for this is that the sulfating supports act as sulfur sinks and thus limit the formation of inactive PdSO_x species [12,16]. On the other hand, regeneration of the activity after SO₂ poisoning appears to be easier for non-sulfating supports since less sulfur species spillover from the support to the PdO [12].

The CH₄ oxidation over zeolite supported Pd has been investigated in many studies, however only a few studies concern the effect of the SAR of the zeolite. These studies show that Pd supported on highly siliceous zeolites has high CH₄ oxidation activity [20,21] together with high resistance against water deactivation [21]. However, to our

knowledge there are no studies in which the influence of SO₂ with respect to silica to alumina ratio for Pd supported on siliceous zeolites was investigated. Therefore, in this study we have aimed to fundamentally investigate the CH₄ oxidation activity over different zeolites with varying SAR in the presence of both water vapor and SO₂. The catalyst samples have also been thoroughly characterized with XRD, STEM, BET, TPO, CH₄-TPR, ICP-SFMS and DRIFTS in addition to activity tests in a flow reactor.

2. Experimental

2.1. Catalyst preparation

NH₄-beta zeolite (Zeolyst International, CP814C) was calcined at 500 °C for 5 h in order to obtain H-beta. The SAR (molar ratio of SiO₂/Al₂O₃) was determined to be 40 with ICP-SFMS (Inductively Coupled Plasma Sector Field Mass Spectrometry), hence this zeolite support will be referred to as 'B40'. Highly siliceous H-beta zeolite was obtained by dealumination with an oxalic acid solution at elevated temperature. A 3 M oxalic acid solution was prepared (10 mL oxalic acid solution/g zeolite) by adding oxalic acid (Sigma-Aldrich, 194131-1KG) to milliQ H₂O and heating it to 70 °C during continuous stirring. After temperature stabilization, the powder form zeolite H-beta (Zeolyst International, CP811C-300, SAR = 300) was added to the acid solution. The slurry was thereafter vigorously stirred for 16 h at 70 °C before it was cooled down. Subsequently, the zeolite powder was separated from most of the acid solution by centrifugation and washed thoroughly with milliQ H₂O followed by drying at 80 °C in an oven overnight and calcination at 500 °C for 5 h. The remaining content of alumina and silica in the zeolite framework was determined with ICP-SFMS analysis giving SAR = 511. Therefore, this dealuminated beta sample will be referred to as 'B511'. A second dealuminated beta sample was prepared in the same way as B511, except for the dealumination time which was increased to 7 days for this sample. The SAR was determined to be 969, also with ICP-SFMS, and will consequently be referred to as 'B969'.

Zeolite SSZ-13 was prepared from zeolite Y based on the method described by McEwen et al. [26] and Olsson et al. [27]. Firstly, 196 mL of 1 M NaOH was prepared by adding NaOH pellets (Sigma-Aldrich, S5881-1KG) to milliQ H₂O followed by stirring for approximately 15 min. Thereafter, 245 g of sodium silicate solution (Sodium silicate in aqueous solution, VWR chemicals, 28079.320) and further 314 g of milliQ H₂O was added and stirred for another 15 min. Subsequently, 24.5 g of zeolite H-Y (Zeolyst International, CBV780, SAR = 80) was added to the solution and a homogenous slurry was obtained by stirring for 30 min. Finally, 103 g of structure directing agent solution, TMAAI (Adamantium hydroxide, ZeoGen SDA 2825, Sachem), was added and stirred for another 30 min. At this point, the entire slurry was transferred and equally divided into four Teflon lined autoclaves. The autoclaves were put into an oven holding 140 °C for 6 days. Thereafter, all autoclaves were removed from the oven and cooled down to room temperature. The zeolite powder was separated from the liquid and thoroughly washed with milliQ H₂O using a centrifuge. The washed powder was dried in an oven at 80 °C. Subsequently, the amorphous zeolite powder was crystallized in an oven for 8 h at 550 °C (heating ramp: 0.5 °C/min). The obtained Na-SSZ-13 was ion-exchanged with 2 M NH₄NO₃ solution (100 mL NH₄NO₃ solution /3 g of Na-SSZ-13), prepared from NH₄NO₃ (ammonium nitrate 98%, ACS reagent, Acros Organics) and milliQ H₂O. After addition of the Na-SSZ-13 powder to the NH₄NO₃ solution, the slurry was put in an oil bath which subsequently was heated to 80 °C during continuous stirring. The slurry was kept heated and agitated for another 15 h and was thereafter removed from the oil bath and cooled down to room temperature. Once again the zeolite powder was thoroughly washed with milliQ H₂O and centrifugation followed by drying at room temperature. The obtained NH₄-SSZ-13 was calcined at 500 °C for 5 h in order to obtain H-SSZ-13. The SAR was determined to be 43 by ICP-SFMS. This zeolite support will be

referred to as ‘S43’.

Another batch of SSZ-13 with higher SAR was prepared using dealuminated zeolite Y. Zeolite H-Y (Zeolyst International, CBV780, SAR = 80) was dealuminated during 16 h using the same procedure as previously described for dealumination of beta zeolite, except that a 1.5 M oxalic acid solution was used. The obtained dealuminated H-Y zeolite powder was then used to produce siliceous H-SSZ-13, according to the same procedure as described previously. The SAR of the final H-SSZ-13 was determined to be 52 with ICP-SFMS, and will be denoted ‘S52’.

As a reference support, Al_2O_3 powder (Sasol, Puralox, SBa-200) was calcined at 700 °C for 2 h. The $\gamma\text{-Al}_2\text{O}_3$ support will be referred to as ‘Al’.

The incipient wetness impregnation method was used to add 1 wt.% Pd to the prepared supports. A solution of $\text{Pd}(\text{NO}_3)_2$ (Heraeus) and milliQ H_2O with a total volume equal to the pore volume of respective support material was prepared. The solution was then added dropwise to the support material and distributed evenly with a spatula. The samples were thereafter dried in an oven at 80 °C overnight, followed by calcination in an oven at 550 °C for 2 h. The final Pd containing samples will be referred to as ‘PdSupport’ (i.e. PdAl, PdB40, PdB511, PdB969, PdS43 and PdS52). All samples were thoroughly pestled with mortar prior to further use.

Washcoated monoliths were prepared for each of the samples and were later used for activity measurements in a flow reactor. All empty monoliths ($\varnothing = 15$ mm, $L = 20$ mm, 400 cpsi) were cleaned in an oven at 600 °C for 2 h prior to washcoating. A slurry containing approximately 90 wt.% liquids (50% ethanol, 50% milliQ H_2O) and 10 wt.% solids (95 wt.% catalyst powder, 5 wt.% binder (Sasol, Dispersal P2)) was prepared. The monolith was dipped in the washcoat slurry and then dried with a heat gun at 90 °C for 4 min while it was rotated continuously in order to distribute the washcoating material evenly in the monolith channels. This procedure was repeated until the total washcoat weight reached 300 +/− 5 mg. The monolith was then calcined for 2 min at 500 °C with the heat gun followed by calcination in an oven at 500 °C for 2 h (ramp: 5 °C/min).

2.2. Characterization

The crystalline structures of the zeolite frameworks of fresh zeolite supports were studied with XRD (X-ray diffraction) using a Siemens D5000 diffractometer operated at 40 kV and 40 mA. Diffraction spectra were collected in the 2θ-interval of 5°–40°. The 2θ increment was set to 0.03°/1 s for the SSZ-13 supports and to 0.02°/1.5 s for the beta supports.

The specific BET surface area of the fresh catalyst samples was measured with N_2 physisorption using a TriStar 3000 instrument. Prior to the physisorption, the samples were degassed in N_2 at 240 °C for 4 h.

The Pd particle size and distribution were investigated with STEM (Scanning Transmission Electron Microscopy). The analysis was performed on catalyst powder which was collected from the monoliths previously used for the activity tests and from monoliths which only had been degreened and pre-treated (see Section 2.4). The powders were distributed onto carbon coated copper grids and were thereafter imaged using a FEI Titan 80–300 equipped with a probe Cs-corrector and a high-angle annular dark-field (HAADF) detector. The microscope was operated in the STEM mode and an acceleration voltage of 300 kV was used.

2.3. Temperature programmed oxidation (TPO) and reduction with CH_4 ($\text{CH}_4\text{-TPR}$)

TPO and $\text{CH}_4\text{-TPR}$ analyses were performed with a Setaram Sensys DSC (Differential Scanning Calorimeter) and Hiden HPR-20 QUI MS (Mass Spectrometer). Fresh catalyst powder, weighed to 100 mg, was put on a sintered, porous quartz bed inside a vertical quartz tube ($\varnothing = 5$ mm). The total flow through the sample tube was 20 mL/min

and Ar was used as the inert carrier gas. Multiple MFC:s (Mass Flow Controllers, Bronkhorst) were used to regulate the flows of the individual gases and the inlet feed to the sample tube. All the samples were degreened prior to the experiments according to the following sequence:

- (1) reduction in 2 vol.% H_2 at 500 °C for 30 min;
- (2) exposure to 0.05 vol.% CH_4 and 5 vol.% O_2 at 600 °C for 60 min;
- (3) reduction in 2 vol.% H_2 at 600 °C for 20 min;
- (4) repetition of step (2).

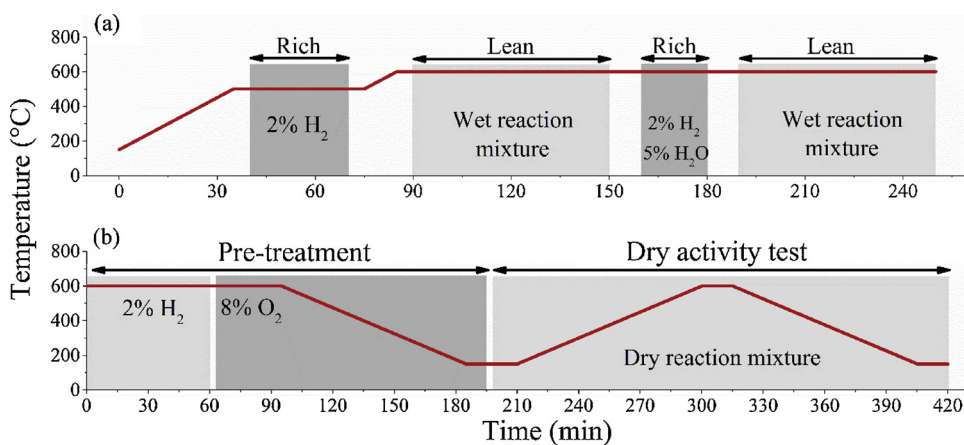
The consecutive pre-treatment consisted of the two following steps:

- (1) oxidation in 5 vol.% O_2 at 600 °C for 30 min;
- (2) reduction in 2 vol.% H_2 at 600 °C for 60 min and cooling to 25 °C (5 °C/min) in the same reducing gas mixture.

The pre-treatment was followed by TPO which was conducted with a gas feed containing 0.05 vol.% O_2 during the entire TPO sequence. The temperature was firstly kept constant at 25 °C during 60 min, in order to ensure a stable O_2 level measured by the MS before initiation of the temperature ramp. The temperature was thereafter ramped up to 600 °C with a heating rate of 10 °C/min. Subsequently, the temperature was kept constant at 600 °C for 20 min, before it was ramped down to 100 °C with a cooling rate of 10 °C/min which ends the TPO sequence. The samples were thereafter pre-treated in 5 vol.% O_2 at 600 °C for 30 min and cooled to 25 °C, also in 5 vol.% O_2 . After this point, the gas feed was changed to 0.05 vol.% CH_4 , which was kept during the entire $\text{CH}_4\text{-TPR}$ sequence. After introducing CH_4 , the temperature was kept constant at 25 °C for 60 min, to ensure a stable CH_4 signal in the MS before the temperature increase. This was followed by a temperature ramp to 600 °C (10 °C/min) and temperature stabilization at 600 °C for 20 min. After the $\text{CH}_4\text{-TPR}$ sequence the sample was flushed with Ar for 5 min and then 0.05 vol.% O_2 for 30 min, also at 600 °C. This latter O_2 step was conducted in order to oxidize coke, which may have been formed on the catalyst surface during the $\text{CH}_4\text{-TPR}$.

2.4. Catalytic activity measurements

Flow reactor experiments were conducted in order to measure the CH_4 oxidation activity for each sample under various conditions. The monolith was wrapped in quartz wool and inserted in a quartz tube ($\varnothing = 16$ mm). The quartz tube was surrounded by a heating coil connected to a power aggregate. The temperature was monitored and controlled by a Eurotherm temperature controller and a thermocouple positioned 10 mm upstream the monolith. A second thermocouple was positioned centrally in the monolith. All data herein presented has been correlated to the temperature measured by the latter mentioned thermocouple. Furthermore, the quartz tube and the heating coil were covered with insulation wool. The water vapor used in the flow reactor experiments was obtained from a CEM system (Controlled Evaporation Mixer, Bronkhorst). The outlet gases from the reactor setup were analyzed with an FTIR (Fourier Transform Infrared Spectroscopy) spectrometer (MKS MultiGas 2030 HS FTIR). The gas flows were regulated by multiple MFC:s (Bronkhorst). For all the experiments, Ar was used as the inert carrier gas and the total gas flow was 800 mL/min (space velocity: 13 600 h^{-1}). In the descriptions of the flow reactor experiments, the inlet gas feed compositions will be denoted as ‘dry reaction mixture’ (0.05 vol.% CH_4 and 8 vol.% O_2 in Ar) and ‘wet reaction mixture’ (0.05 vol.% CH_4 , 8 vol.% O_2 and 5 vol.% H_2O in Ar). For clarity, sudden spikes in the data due to occasional water condensation in the CEM system have been removed from all activity data presented in this paper. This does not affect any experimental conclusions, however, original figures without data removal are available in Figure S2 - Figure S5 (Supplementary Material).



2.4.1. Degreening and pre-treatment

Each monolith was degreened once prior to any of the experiments and pre-treated before each experiment. The degreening was performed according to the following procedure (which also is illustrated in Fig. 1a):

- (1) reduction in 2 vol.% H₂ at 500 °C for 30 min;
- (2) exposure to the wet reaction mixture at 600 °C for 60 min;
- (3) exposure to 2 vol.% H₂ and 5 vol.% H₂O at 600 °C for 20 min;
- (4) repetition of step (2).

The pre-treatment, which also is shown schematically in Fig. 1b and Fig. 2a, was conducted in two steps:

- (1) reduction in 2 vol.% H₂ at 600 °C for 60 min;
- (2) oxidation in 8 vol.% O₂ at 600 °C for 30 min and cooling to 150 °C (5 °C/min) in the same oxidizing gas mixture.

2.4.2. Dry activity test

In the first flow reactor experiment, which followed directly after the degreening and the pre-treatment, the CH₄ oxidation activity was tested in the dry reaction mixture, *i.e.* in the absence of water vapor. The reactor temperature was programmed as following: ramp up (5 °C/min) from 150 °C to 600 °C; temperature stabilization at 600 °C for 15 min; ramp down from 600 °C to 150 °C; temperature stabilization at 150 °C for 15 min. The reactor chamber was provided with the dry reaction mixture during the entire sequence. The procedure for this experiment is illustrated in Fig. 1b.

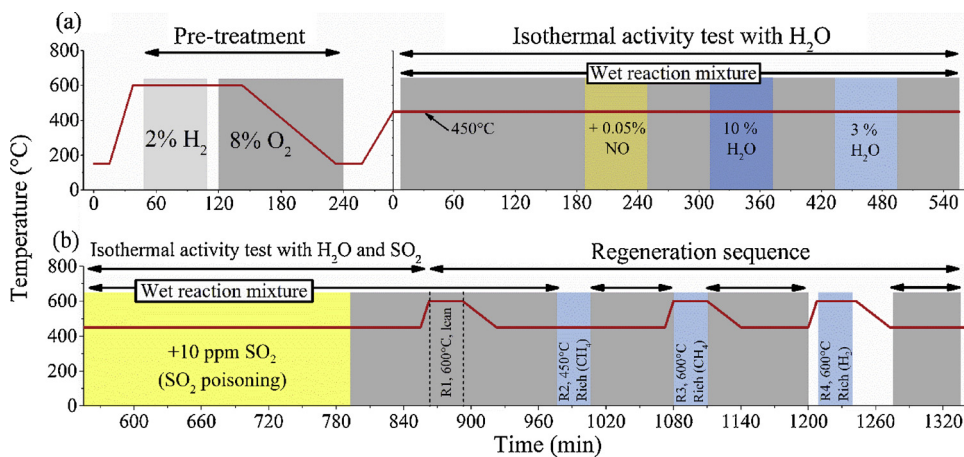


Fig. 1. Illustration of the experimental procedures for the degreening (a) and the pre-treatment together with the subsequent dry activity test (b). Dry reaction mixture corresponds to an inlet gas feed containing 0.05 vol.% CH₄ and 8 vol.% O₂ and wet reaction mixture corresponds to 0.05 vol.% CH₄, 8 vol.% O₂ and 5 vol.% H₂O.

2.4.3. Isothermal activity test with H₂O

The catalytic activity was also tested in the presence of water vapor under isothermal conditions. This flow reactor experiment will be referred to as the ‘isothermal activity test with H₂O’ and is schematically illustrated in Fig. 2a. Prior to this test, all samples were once again pre-treated according to procedure in Section 2.4.1. Subsequently, the temperature was increased from 150 °C to 450 °C in Ar followed by the introduction of the wet reaction mixture, which was the starting point of the isothermal activity test. The temperature was kept constant at 450 °C for 9 h while the inlet gas composition was varied according to the following scheme:

- (1) wet reaction mixture for 3 h;
- (2) wet reaction mixture + 0.05 vol.% NO for 1 h;
- (3) wet reaction mixture for 1 h;
- (4) wet reaction mixture but with higher water vapor concentration (10 vol.% water vapor) for 1 h;
- (5) wet reaction mixture for 1 h;
- (6) wet reaction mixture but with lower water vapor concentration (3 vol.% water vapor) for 1 h;
- (7) wet reaction mixture for 1 h.

2.4.4. Isothermal activity test with H₂O and SO₂

The ‘isothermal activity test with H₂O and SO₂’ was followed immediately after the ‘isothermal activity test with H₂O’ (Section 2.4.3) by adding 10 ppm SO₂ to the wet reaction mixture, *i.e.* no pre-treatment was performed prior to this step. Instead, the temperature was kept at 450 °C for another 5 h during this entire sequence. Fig. 2b shows a schematic illustration of this sequence, which was performed in the following steps:

Fig. 2. Illustration of the experimental procedures for the pre-treatment together with the isothermal activity test with H₂O (a) and the isothermal activity test with H₂O and SO₂ together with the regeneration sequence (b). Wet reaction mixture corresponds to an inlet gas feed containing 0.05 vol.% CH₄, 8 vol.% O₂ and 5 vol.% H₂O. Modifications of the inlet gas feed composition are given in the figure.

Table 1

Sample information: Pd loading, SAR, Pd/Al ratio, Na content and specific BET surface area of respective fresh sample.

Sample	Pd content (wt. %) ^a	SAR (molar ratio $\text{SiO}_2/\text{Al}_2\text{O}_3$) ^a	Pd/Al (molar ratio) ^a	Na content (wt. %) ^a	BET surface area (m^2/g)
PdAl	0.97	–	–	–	177.2
PdB40	0.92	40	0.14	< 0.08	603.9
PdB511	1.05	511	1.96	< 0.08	612.9
PdB969	1.00	969	3.81	< 0.1	553.4
PdS43	1.02	43	0.16	< 0.09	775.8
PdS52	1.06	52	0.26	< 0.1	713.9

* Data obtained from ICP-SFMS analysis.

- (1) wet reaction mixture + 10 ppm SO_2 for 4 h (SO_2 poisoning step);
(2) wet reaction mixture for 1 h.

In addition, another monolith was also prepared and exposed to similar conditions and thereafter analyzed with ICP-SFMS in order to quantify the amount of sulfur stored on the sample after SO_2 poisoning. The exact conditions for this were (1) degreening and pre-treatment at 600 °C (Section 2.4.1); (2) wet reaction mixture for 1 h at 450 °C; (3) wet reaction mixture + 10 ppm SO_2 for 4 h at 450 °C (SO_2 poisoning step); (4) cooling to room temperature in Ar.

2.4.5. Regeneration sequence

The isothermal activity test with H_2O and SO_2 was immediately continued by a sequence of regeneration steps, in order to evaluate the possibility to regenerate the catalytic activity after deactivation with SO_2 and water vapor. The ‘regeneration sequence’, which is shown in Fig. 2b, was conducted with four regeneration steps (R1, R2, R3 and R4) with CH_4 oxidation in wet reaction mixture at 450 °C for 1 h in between, i.e. the following scheme was repeated four times: (1): RX, where X is the number of regeneration, X = 1–4; (2) CH_4 oxidation in wet reaction mixture at 450 °C for 1 h.

The first regeneration (R1) was conducted entirely in the wet reaction mixture while the reactor temperature programmed according to (a) ramp up (20 °C/min) from 450 °C to 600 °C; (b) 30 min isotherm at 600 °C; (c) ramp down (5 °C/min) from 600 °C to 450 °C. The second regeneration step (R2) was conducted isothermally at 450 °C for 30 min with a rich inlet gas feed containing 0.05 vol.% CH_4 and 5 vol.% H_2O . The third regeneration step (R3) was identical to R1 except that the reactor chamber was provided with a rich inlet gas feed (0.05 vol.% CH_4 , 5 vol.% H_2O) in step (b). Finally, the forth regeneration step (R4) was performed in the following steps (a) ramp up (20 °C/min) from 450 °C to 600 °C in and 10 min temperature stabilization in Ar; (b) 30 min isotherm at 600 °C in 2 vol.% H_2 and 5 vol.% H_2O ; (c) ramp down (5 °C/min) from 600 °C to 450 °C and 10 min temperature stabilization in Ar. When the regeneration sequence was finished, the samples were cooled in Ar and thereafter analyzed with ICP-SFMS in order to see how much sulfur that was remaining on the samples.

2.5. DRIFTS experiments

The DRIFTS (Diffuse Reflectance Infrared Fourier Transform Spectroscopy) analysis was conducted with a Vertex 70 spectrometer equipped with a liquid nitrogen cooled MCT (Mercury Cadmium Telluride) detector. A sieved fraction of the catalyst powder in the range of 40–80 μm was put into the reaction cell (High Temperature Reaction Chamber, Harrick Praying Mantis) equipped with CaF_2 windows. The temperature in the reaction cell was measured and controlled with a thermocouple connected to a Eurotherm controller. The total gas flow through the cell was kept constant to 100 mL/min and the each of the individual gases, including Ar which was used as the carrier gas, was dosed by separate MFCs (Bronkhorst). The absorption spectra were

collected in the wavenumber range of 400–4000 cm^{-1} with a spectral resolution of 4 cm^{-1} .

Before the catalyst powders were put in the DRIFTS cell, they were all thermally treated in air at 600 °C for 2 h (heating ramp 5 °C/min). Subsequently, the powder was put in the cell and degreened at 550 °C according to the following procedure (1) reduction in 2 vol.% H_2 for 30 min; (2) exposure to lean conditions (0.05 vol.% CH_4 , 8 vol.% O_2 and 2 vol.% H_2O) for 60 min. The samples were thereafter pre-treated, also at 550 °C, first in 2 vol.% H_2 for 30 min followed by 8 vol.% O_2 for 30 min. After this point, the temperature was decreased to 80 °C in Ar only during 2 h to ensure stable temperature before initiation of the experiments. The background spectra were acquired in the end of this step, i.e. at 80 °C in Ar. After this step, the reaction chamber was provided with 0.1 vol.% NO for 60 min at 80 °C. The spectra herein presented were recorded during the last minute of the NO exposure step and are background corrected.

3. Results and discussion

3.1. Characterization

The Pd content, SAR and the Na content of the samples were determined by ICP-SFMS and are displayed in Table 1. It can be seen that the Pd content for all samples was around 1 wt.% and that the Na content was below the detection limit of the ICP-SFMS measurement. Moreover, the SAR, i.e. the molar ratio of $\text{SiO}_2/\text{Al}_2\text{O}_3$, was widely spread from 40 to 969 for the beta samples, whereas the SAR of SSZ-13 was 43 and 52. There are several reasons which could explain the higher SAR of the beta zeolite samples. Firstly, the beta samples were dealuminated with higher oxalic acid concentration and in addition the dealumination time was also greatly increased for the B969 support. Secondly, Y zeolite was dealuminated prior to synthesis of SSZ-13, whereas the beta samples were dealuminated as such. In addition, it has previously been shown that the structure of beta zeolite is favorable for efficient dealumination with acids [28]. Moreover, it should be noted that ICP-SFMS only gives information of the total alumina content, i.e. it cannot be distinguished with this method whether the alumina is part in the zeolite framework or exists as extra-framework alumina [28]. However, acidic treatment of zeolites has been reported to efficiently remove non-framework alumina [29,30]. Thus, this may apply also for the samples in this study but have not been studied in detail. The dealumination treatment did not result in any significant decrease in the BET surface area, Table 1, although the BET surface area for the most dealuminated sample (PdB969) decreased to some extent. Moreover, the crystallinity of zeolites was preserved based on the XRD patterns shown in Figure S1 (Supplementary Material). Thus, the zeolite frameworks appear to remain fairly intact despite the acidic dealumination. The BET surface area was the highest for SSZ-13 followed by the beta supports, whereas the $\gamma\text{-Al}_2\text{O}_3$, naturally, had significantly lower surface area, see Table 1.

STEM images were collected for PdB40 and PdB511 in order to study how the size and the distribution of the Pd particles are influenced by the SAR of the zeolite support, see Fig. 3. As a reference, also the corresponding images of PdAl are presented in Figure S7 (Supplementary Material). Fig. 3a and c show the catalysts prior to the activity tests (i.e. after the degreening and the pre-treatment), whereas Fig. 3b and d represent the spent catalysts after the activity tests. It should be noted that in addition to the Pd particles, cationic Pd^{2+} species, which cannot be distinguished in the STEM images, may exist on the acidic sites in the zeolite framework. PdB40, Fig. 3a and b, exhibits a high number of small and well dispersed Pd particles with a diameter typically < 6 nm. Hence, a large fraction of the particles are considerably larger than the channels in zeolite beta framework and must therefore be located on the external areas of the zeolite. However, it cannot be completely excluded that particles which are small enough to be contained inside the zeolite framework, and therefore are difficult to

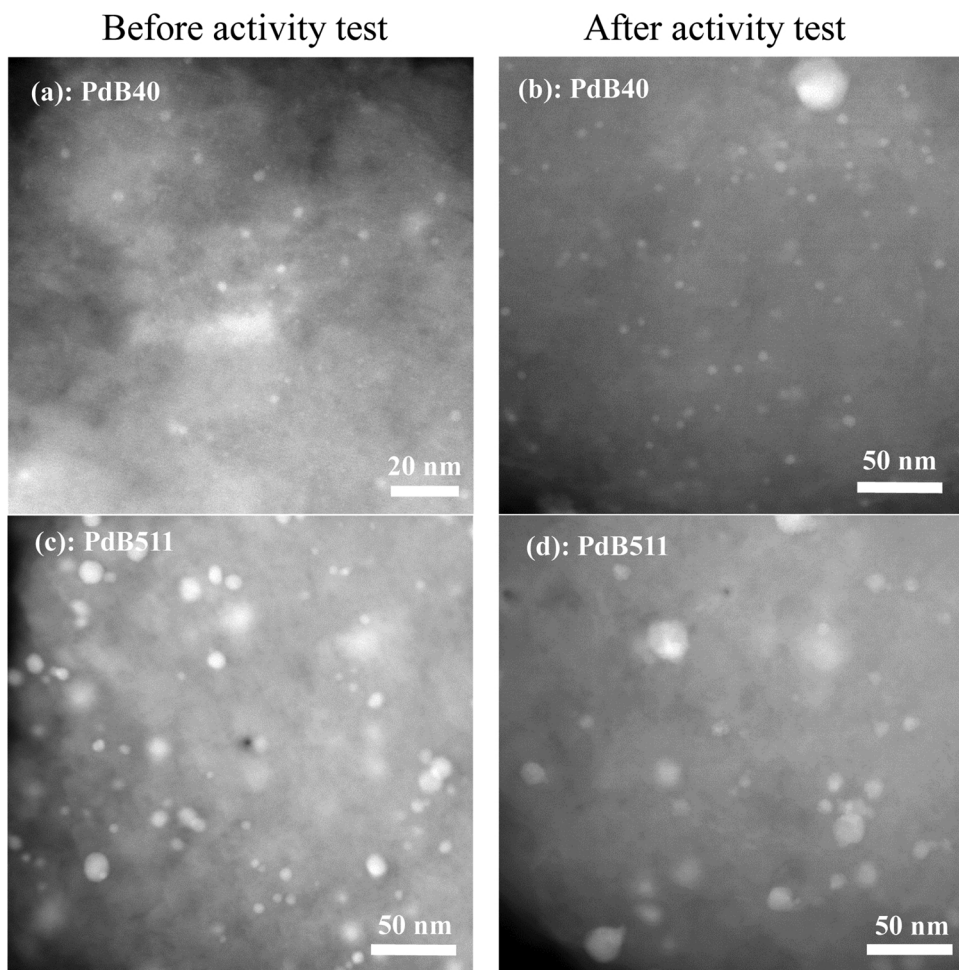


Fig. 3. STEM images of PdB40 (a,b) and PdB511 (c,d). The images to the left (a,c) were acquired of the samples before the activity test (i.e. after the degreening and the pre-treatment), whereas the images to the right (b,d) show the samples after the activity tests and the regeneration sequence.

detect, also exist. In addition, there are a few considerably larger Pd particles with diameters in the range of approximately 10–60 nm. Due to their large size, these particles are undeniably also located on the external surfaces of the zeolite framework. The images of PdB511, Fig. 3c and d, are rather different from those of PdB40. The fraction of small particles, which clearly could be distinguished in the PdB40 sample, is almost completely absent in PdB511. By contrast, PdB511 contains less dispersed Pd particles with typical diameters of 5–20 nm, however in addition to less frequent larger particles with diameters up to approximately 40 nm. Judged from the particle size, these particles are also positioned externally on the zeolite. Neither of the samples showed any obvious signs of Pd particle sintering by comparison of the STEM images acquired before and after the activity tests in Fig. 3, although a smaller degree of sintering cannot be excluded. However, it is clear that a higher SAR of the beta zeolite support resulted in the formation of larger Pd particles. Thus, the SAR has a significant impact on the Pd distribution and Pd particle formation. This observation agrees well with previous studies which report that the lower number of acidic sites in zeolites with high SAR results in the formation of larger particles, whereas the formation of highly dispersed Pd particles and/or monoatomic Pd^{2+} species are favored with decreasing SAR due to the interactions between the basic Pd and the higher number of acidic sites [21,31].

Besides SAR, several other factors have been pointed out to influence the Pd dispersion and the amount of ion-exchanged Pd^{2+} in zeolite supported Pd catalysts. For instance, a low Pd loading results in higher Pd dispersion and more Pd^{2+} species, whereas a high Pd content

facilitates the formation of Pd particles [31–33]. However, it is likely that the Pd/Al ratio is the important factor for what type of Pd species are formed, rather than the SAR and Pd loading separately [31]. Furthermore, it has been shown that Pd reversibly rearranges into large clusters in a reducing atmosphere and disperses into smaller particles and monoatomic Pd^{2+} species in an oxidizing gas mixture [33–35]. Moreover, it has also been reported that PdO can be converted into ion-exchanged Pd^{2+} species when the zeolite is in its hydrogen form but not in its sodium form [34] and that Pd sintering can be mitigated by fully ion-exchange the zeolite with sodium [22]. In addition, the treatment of the sample is important, for instance hydrothermal ageing results in more ion-exchanged Pd^{2+} species and fewer Pd particles [31,36]. Ryou et al. [36] reported that the PdO particles in fresh Pd/SSZ-13 ($\text{Si}/\text{Al} = 22.4$) rearrange into small, dispersed PdO particles and monoatomic Pd^{2+} upon hydrothermal ageing at 750°C for 25 h. It was also seen that this effect falls off with higher Pd loadings and that ageing at high temperature is not enough to form the Pd^{2+} species, but also the presence of water vapor is required.

The different types of Pd species present in the samples were further investigated with DRIFTS after 60 min of exposure to 0.1 vol.% NO at 80°C . The backgrounds were acquired at 80°C in Ar and are subtracted from all spectra shown in Fig. 4. The exposure of NO to Pd/zeolite samples results in the formation of nitrosyl groups on isolated Pd^{2+} atoms [36–40], hence NO-DRIFTS can be used to confirm or deny the presence of Pd^{2+} species. However, the existence of PdO particles is not possible to distinguish from the NO-DRIFTS data, due to their low ability to NO adsorption [32,36,41].

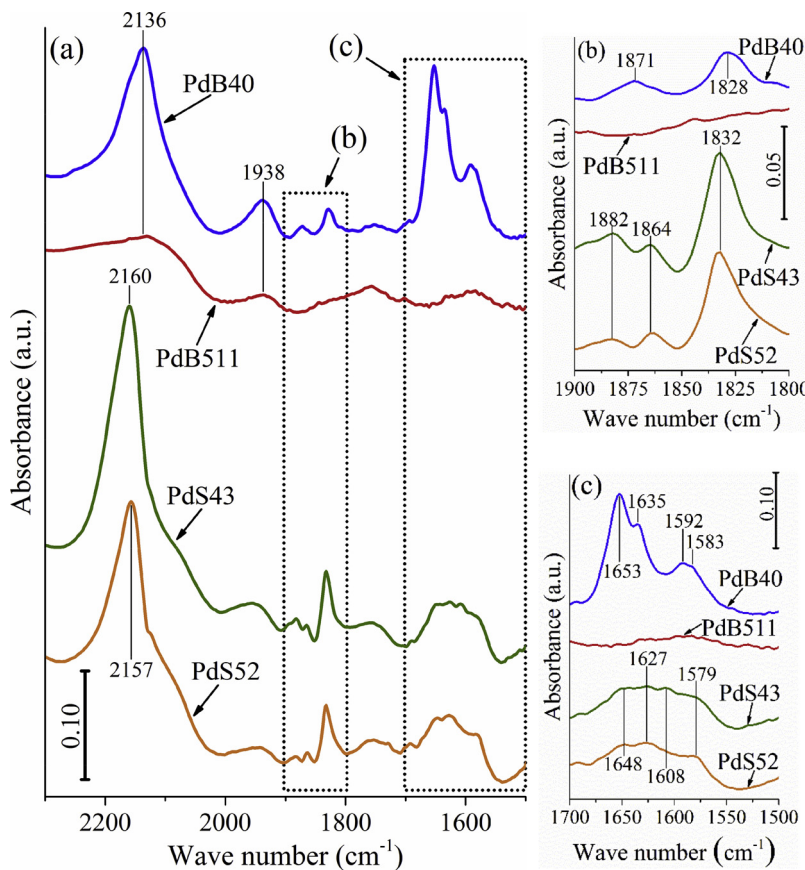


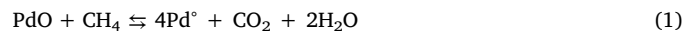
Fig. 4. DRIFTS spectra collected after 60 min exposure to 0.1 vol. % NO in the wave number region 2300–1500 cm^{−1} for the zeolite samples (a) and the magnification of the regions 1900–1800 cm^{−1} (b) and 1700–1500 cm^{−1} (c). From bottom to top: PdS52 (orange line), PdS43 (green line), PdB511 (red line) and PdB40 (blue line). (For interpretation of the references to colour in this figure legend, the reader is referred to the web version of this article).

There were significant differences in the spectra of the zeolite samples. The first pronounced difference is the absorbance peaks at around 2160–2136 cm^{−1} for PdB40, PdS43 and PdS52 (Fig. 4a). These peaks are ascribed to IR absorbance of NO⁺ on the Brønstedt acidic sites in the zeolite networks, which previously have been observed in the wavenumber region of 2220–2128 cm^{−1} for different types of zeolites [37–39,42,43]. By contrast, PdB511 shows much less absorbance in this region, which confirms the low number of acidic sites within the highly siliceous zeolite framework. Furthermore, the existence of monoatomic Pd²⁺ in zeolite supported samples can be recognized by the formation of nitrosyl species with the corresponding absorbance in the region of 1800–1881 cm^{−1} [36–40] for different zeolite frameworks. Thus, the features in Fig. 4b at 1871 and 1828 cm^{−1} for PdB40 as well as 1882, 1864 and 1832 cm^{−1} for PdS43 are ascribed to nitrosyl species on the ion-exchanged Pd²⁺. The PdB511 is also characterized by the absence of absorbance in this wavenumber region. Hence, the low number of acidic sites in the B511 framework prevents the formation of ion-exchanged Pd²⁺ species which suggests that an increased SAR favors the formation of Pd particles.

The third region of interest is the region of 1700–1500 cm^{−1} which is presented in Fig. 4c. Also in this region, the spectrum of PdB511 was almost flat. On the contrary PdB40 expressed a distinct peak at 1653 cm^{−1} with clear shoulder peaks at 1635, 1592 and 1583 cm^{−1}. Furthermore, the SSZ-13 supported samples showed broad absorbance bands with weak maxima at around 1648, 1627, 1608 and 1579 cm^{−1}. Several authors have ascribed absorption bands in this region to nitrates [37,44,45]. Adsorbed water has also been reported to have one absorption band at 1623 cm^{−1} [43], however, since no water vapor was added or formed as a reaction product, this is unlikely to contribute to bands in Fig. 4c. Moreover, gaseous NO₂ has characteristic IR absorbance at 1628 and 1609 cm^{−1} and adsorbed NO₂ at 1671 cm^{−1} [37]. However, since O₂ was not present during the NO adsorption, not much NO₂ is expected to be formed. Thus, we suggest that the bands in the

region of 1500–1700 cm^{−1} correspond to nitrates associated to the alumina in the zeolite samples and that much less or no nitrates are formed on highly siliceous zeolites. However, the main conclusion from the NO-DRIFTS is that PdB40, PdS43 and PdS52 contain ion-exchanged Pd²⁺ species, whereas PdB511 primarily contains Pd in the form of particles.

The samples were further characterized with CH₄-TPR and TPO in order to study the reduction and oxidation properties of the Pd species and to assist the interpretation of the catalytic activity results (Section 3.2–3.4). Therefore, the same temperature interval was used for the CH₄-TPR and the TPO as for the catalytic activity experiments, *i.e.* up to 600 °C. The samples were well oxidized prior to the CH₄-TPR, which was initiated by the introduction of CH₄ at room temperature followed by linearly increased temperature to 600 °C. The CH₄-TPR profiles for all samples are displayed in Figs. 5–7. The reduction of PdO with CH₄ results in the production of CO₂ and H₂O, which is shown in Reaction 1 [46]. However, as the temperature increases and the Pd becomes fully reduced, CH₄ will instead be consumed in the steam reforming reaction (Reaction 2), the water gas shift reaction (Reaction 3) and due to coke formation (Reaction 4) [46].



PdAl was studied as a reference material to compare with different Pd/zeolites and the CH₄-TPR result for PdAl is displayed in Fig. 5. The CH₄ consumption peak at 196 °C corresponds to the PdO reduction, which is consistent with our previous works [46–48]. At higher temperatures, the CH₄ was completely consumed by the steam reforming reaction, the water gas shift reaction and coke formation (Reaction 2–4)

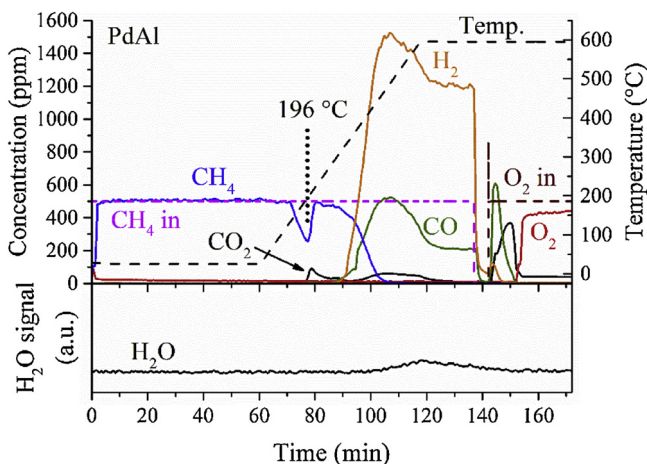


Fig. 5. CH₄-TPR conducted with 0.05 vol.% CH₄ and a temperature ramp of 10 °C/min for PdAl.

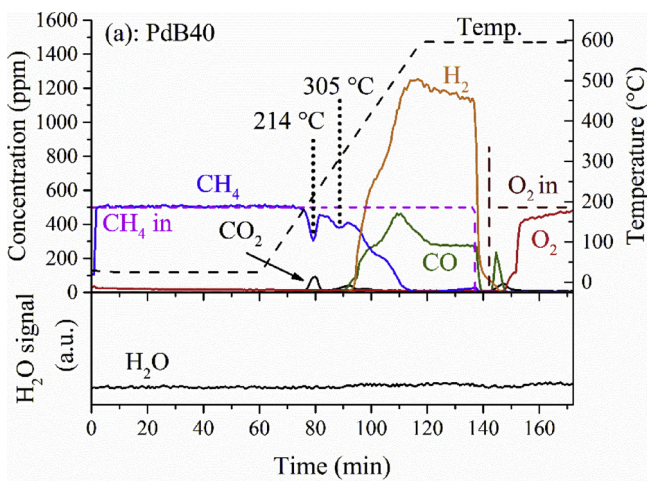


Fig. 6. CH₄-TPR conducted with 0.05 vol.% CH₄ and a temperature ramp of 10 °C/min for PdB40 (a) and PdB511 (b).

with resulting production of H₂, CO and CO₂. The formation of surface coke was further proven by the formation CO and CO₂ production during the O₂ step subsequent to the CH₄-TPR.

Fig. 6a presents the CH₄-TPR for PdB40 where the negative peak at around 214 °C represents the reduction of PdO. The simultaneously formed CO₂ was detected by the mass spectrometer, whereas no increase in the H₂O concentration was recorded, assumingly due to water

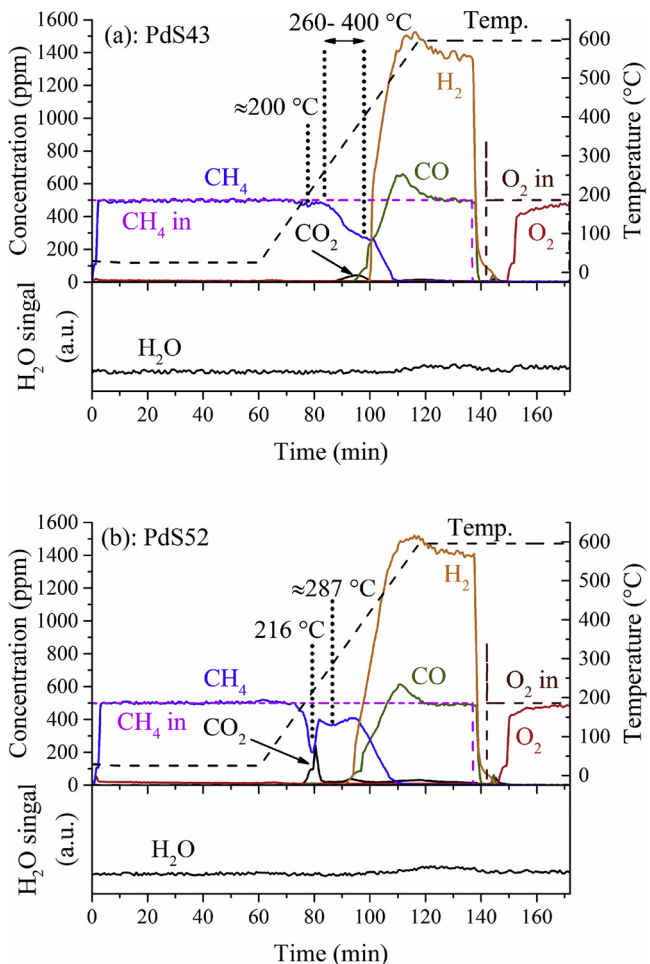


Fig. 7. CH₄-TPR conducted with 0.05 vol.% CH₄ and a temperature ramp of 10 °C/min for PdS43 (a) and PdS52 (b).

adsorption on the catalyst surface. The weak negative peak at approximately 305 °C may correspond to the reduction of PdO species, but this CH₄ consumption may also have been a result of the steam reforming reaction, the water gas shift reaction and/or due to coke formation. However, the formation H₂ and CO was observed first at slightly higher temperatures, which argues for that this negative peak originates from the reduction of PdO species. Moreover, the existence of two reduction peaks is supported by previous findings with H₂-TPR for Pd/beta, where the reduction peak at lower temperatures was assigned to the reduction of PdO and the peak at higher temperatures was ascribed to the reduction of PdO₂ and/or ion-exchanged Pd²⁺ species [25,49]. Interestingly, PdB511 exhibits only one single, sharp reduction peak at 223 °C (Fig. 6b). Furthermore, the existence of Pd²⁺ species could be confirmed with NO-DRIFTS in PdB40 but not in PdB511 (Fig. 4). Thus, this argues for that the second peak at 305 °C in the CH₄-TPR profile for PdB40 corresponds to the reduction of Pd²⁺ species, whereas the peaks at 214 °C for PdB40 and at 223 °C for PdB511 are assigned to the reduction of PdO particles. These results are also consistent with the experiment on PdAl, where the reduction of PdO particles occurred in a similar temperature range (196 °C), see Fig. 5. The slightly lower temperature for PdAl could be due to different particle sizes and/or slightly different interactions with the support. Furthermore, it can also be seen that the H₂O concentration rapidly increased simultaneously as the reduction of the PdO particles for PdB511 but not for PdB40. This is assumingly a result of the low water adsorption on the hydrophobic PdB511 and the higher water adsorption capacity of PdB40. Another observation from Fig. 6a and b is that more CO and CO₂ was formed during the O₂ step subsequent to the CH₄-TPR for PdB511

than for PdB40. This indicates that coke formation is facilitated by increased SAR of the zeolite support which may be related to the larger Pd particles. This information should be considered for instance in the case of regeneration in reducing conditions, which thus can result in a coke coverage of active sites and decreased catalytic activity. After CH₄ reduction of the catalyst, it is therefore important to treat the catalyst in oxidizing conditions at high temperature to burn off the coke.

The CH₄-TPR profiles for PdS43 (Fig. 7a) and PdS52 (Fig. 7b) show many similarities to the CH₄-TPR profiles of the beta supported samples. The reduction of the PdO particles in PdS43 was expressed as a weakly developed decrease in the CH₄ concentration at approximately 200 °C. The fact that the CH₄ consumption was extremely low indicates that only few PdO particles were present in the PdS43 sample and that it therefore is difficult to precisely determine the reduction temperature of the PdO particles for this sample. In the temperature interval 260–400 °C a further decrease in the CH₄ concentration together with a slight increase of the CO₂ signal was noticed. Since no or very little H₂ and CO was produced in this temperature interval, we believe that this CH₄ consumption corresponds to the reduction of ion-exchanged Pd²⁺ species. Conclusively, most Pd existed as monoatomic Pd²⁺ species in the PdS43 sample, which also is supported by the NO-DRIFTS analysis (Fig. 4). By contrast, a clear peak was developed for the reduction of PdO particles in PdS52 at 216 °C (Fig. 7b). Hence, significantly more PdO particles were present in the PdS52 sample than in the PdS43 sample. However, the shallow dip in the CH₄ concentration at around 287 °C for the PdS52 is most likely due to the reduction of ion-exchanged Pd²⁺ species, since the H₂ and CO production was initiated at slightly higher temperatures. It should also be noted that no increase in the water signal could be detected during the CH₄-TPR sequence for neither the PdS43 sample nor the PdS52 sample, which most likely is a result of water adsorption on the support.

Fig. 8 displays the TPO profiles for the zeolite supported samples. Prior to the TPO, all samples were treated in H₂ to ensure fully reduced Pd before the introduction of O₂. Both of the beta supported samples show one single O₂ consumption peak with a minimum at approximately 454 °C for PdB40 (Fig. 8a) and 359 °C for PdB511 (Fig. 8b). This shows that the SAR of the zeolite also has a significant impact on the oxidation of Pd and that a higher SAR results in a shift towards lower oxidation temperatures. Moreover, the broadly shaped consumption peak for PdB40 shows that the O₂ consumption occurred over a large temperature interval, whereas the PdB511 sample expressed a much sharper peak with very little asymmetry. Both the results from the NO-DRIFTS (Fig. 4) and the CH₄-TPR (Fig. 6) showed that PdB40 contains both Pd particles and ion-exchanged Pd²⁺ species, whereas PdB511 almost exclusively contains Pd in the particle form. Thus, the wide O₂

consumption peak for PdB40 at 454 °C is assigned to oxidation of both Pd particles and ion-exchanged Pd²⁺ species and the peak at 359 °C for PdB511 corresponds to the oxidation of Pd particles.

The same trend was observed for the SSZ-13 supported samples. The PdS43 sample (Fig. 8c) has a shallow O₂ consumption peak at around 456 °C, which most likely corresponds to the oxidation of Pd²⁺ species. It also appears to be a weak peak at 600 °C which shows that some of the Pd species were very difficult to oxidize. Thus, both the TPO and CH₄-TPR indicate that the major part of the Pd is ion-exchanged with the zeolite structure in the PdS43 sample. Contrarily, it can be seen that PdS52 (Fig. 8d) had a sharp peak at 386 °C, although asymmetrically shaped. Thus, it is believed that the O₂ uptake at around 386 °C corresponds to the oxidation of Pd particles, whereas the O₂ uptake at higher temperatures occurred due to oxidation of ion-exchanged Pd²⁺. Hence, both the beta and the SSZ-13 samples showed that an increased SAR results in lower oxidation temperatures of the Pd which is a consequence of less ion-exchanged Pd²⁺ species but also the particle size and differences in Pd-support interactions may have influenced. Moreover, it also appears that the beta supported samples generally have slightly lower oxidation temperatures than the SSZ-13 supported samples. Considering the TPO patterns in Fig. 8, it is also clear that the PdO is stable at temperatures below 600 °C, which is in agreement with the previous studies which showed that the decomposition of PdO occurs at around 700–800 °C [46–48].

3.2. Catalytic activity in the absence of water vapor

The CH₄ oxidation activity was evaluated in a flow reactor using monoliths, washcoated with respective catalyst sample. Prior to the experiment, each monolith was degreened and pre-treated at 600 °C according to the procedure described in Section 2.4.1. The CH₄ oxidation activity in the absence of water vapor was evaluated by providing the reactor with the dry reaction mixture while the temperature was ramped (5 °C/min) from 150 °C to 600 °C, followed by cooling to 150 °C (also 5 °C/min). Based on the CH₄ conversion data shown in Fig. 9 and the corresponding temperature of 50% CH₄ conversion (T_{50%}) presented in Fig. 10, the catalytic activity of the samples in the absence of water vapor decreased in the following order: PdAl > PdB969 > PdB511 > PdB40 > PdS52 > PdS43. Hence, the highest activity was expressed by PdAl, which had a T_{50%} of 271 °C (Figs. 9c and 10), however, also the PdB969 sample provided about same level of CH₄ conversion. In general, the beta supported samples, shown in Figs. 9a and 10, showed a clear trend of higher activity with increasing SAR of the zeolite support. The T_{50%} was 307 °C, 291 °C and 281 °C during the heating ramp for PdB40, PdB511 and PdB969, respectively.

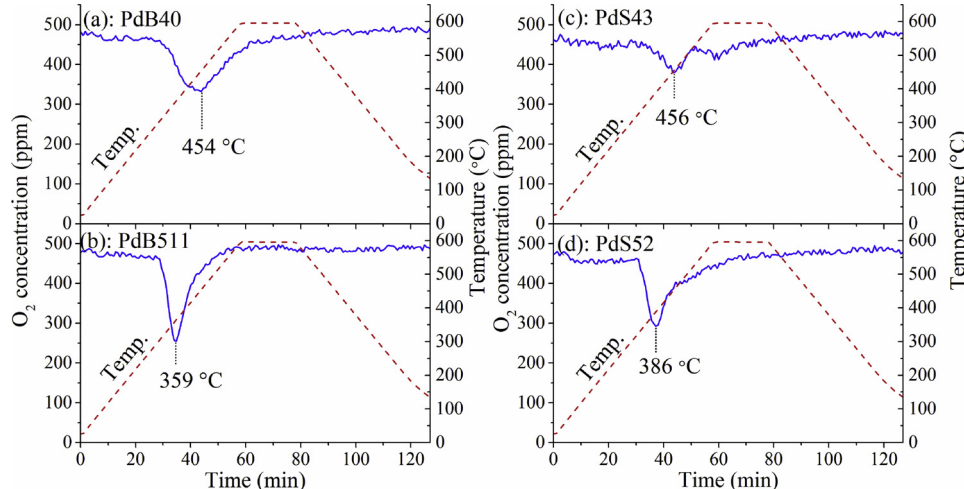


Fig. 8. TPO conducted with 0.05 vol.% O₂ and a temperature ramp of 10 °C/min for PdB40 (a), PdB511 (b), PdS43 (c) and PdS52 (d).

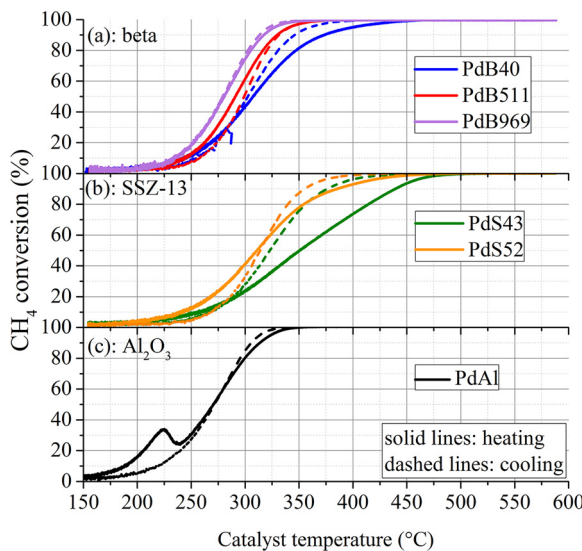


Fig. 9. Dry activity test performed with dry reaction mixture (0.05 vol.% CH₄ and 8 vol.% O₂) for the beta supported samples (a): PdB40- blue line, PdB511- red line, PdB969- purple line; and the SSZ-13 supported samples (b): PdS43- green line, PdS52-orange line; and the PdAl (c)- black line. (For interpretation of the references to colour in this figure legend, the reader is referred to the web version of this article).

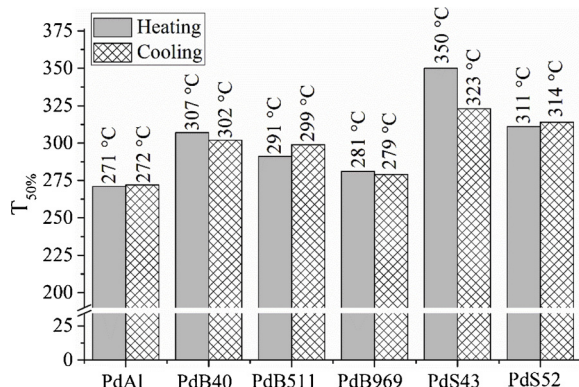


Fig. 10. Temperature of 50% CH₄ conversion (T_{50%}) in the dry reaction mixture (0.05 vol.% CH₄ and 8 vol.% O₂) corresponding to the activity data presented in Fig. 9. From left to right: PdAl, PdB40, PdB511, PdB969, PdS43 and PdS52. Solid bars represent heating and checked bars cooling.

Interestingly, it can also be observed that the hysteresis between the heating and cooling ramp decreases with higher SAR. The PdB40 sample had lower activity during heating than cooling, whereas the PdB511 sample exhibited the opposite and no hysteresis was expressed by the PdB969 sample. The same trends of increased catalytic activity and less hysteresis corresponding to higher SAR were also observed for the SSZ-13 supported samples, Figs. 9b and 10. Both PdS43 and PdS52 showed higher T_{50%}, i.e. lower activity, than any of the beta supported samples. The T_{50%} was 350 °C and 311 °C during the heating ramp for PdS43 and PdS52, respectively. Hence, not only the SAR but also the type of zeolite framework influences the CH₄ oxidation activity under dry conditions. Furthermore, both of the SSZ-13 supported samples showed large hysteresis, in particular the PdS43 sample.

There are many factors that may have contributed to the differences in the catalytic activity and hysteresis seen in Fig. 9. However, since all samples were stabilized in the preceding degreening and pre-treatment (described in Section 2.4.1), structural changes such as sintering, are not likely to cause the hysteresis. Neither is the small amount of water, produced in the CH₄ oxidation reaction, likely to impact the CH₄ oxidation activity to any larger extent. Thus, the most reasonable

explanation for the hysteresis is progressively changed oxidation state of the Pd during the experiment, whereas the decreased hysteresis with higher SAR may be related to the higher content of Pd particles in relation to ion-exchanged Pd²⁺ species. It was shown in the TPO (Fig. 8) that the isolated Pd²⁺ species have much higher temperature of oxidation than Pd particles. Therefore, it is possible that the sample with high content of Pd²⁺ species obtained a more optimal oxidation state first at high temperatures and consequently expressed higher CH₄ oxidation activity during the cooling ramp than during the heating ramp. To summarize, we suggest that the decreased hysteresis and enhanced CH₄ oxidation activity under dry conditions for Pd supported on zeolites with high SAR is a result of:

(i): more Pd particles in relation to ion-exchanged Pd²⁺, which is supported by the results from the NO-DRIFTS (Fig. 4), CH₄-TPR (Figs. 6 and 7) and TPO (Fig. 8).

(ii): formation of more PdO, which was observed from the higher O₂ consumption in the TPO (Fig. 8) and the higher CH₄ consumption in the CH₄-TPR (Figs. 6 and 7).

(iii): decreased oxidation and reduction temperature due to the higher amount of Pd particles in comparison to ion-exchanged Pd²⁺ species.

It should be noted that it is not clear based on the current literature how active the ion-exchanged Pd²⁺ species are for CH₄ oxidation in relation to Pd in its particle form. However, our results show that the CH₄ oxidation activity increases with the SAR and therefore also with an increasing content of Pd particles in relation to ion-exchanged Pd²⁺ species. The sample with the highest SAR, and consequently least monoatomic Pd²⁺, showed about the same activity level as PdAl, which only contains Pd in particle form. Therefore, we suggest that the PdO particles are more active than the ion-exchanged Pd²⁺ species.

3.3. Catalytic activity in the presence of water vapor

The CH₄ oxidation activity was thereafter evaluated in the presences of water vapor, which is known to severely deactivate Pd based catalysts [6]. The isothermal activity test seen in Fig. 11 was conducted at 450 °C while the reactor was provided with different feed gas mixtures. During the first 3 h, the catalyst samples were exposed to the wet reaction mixture (0.05 vol.% CH₄, 8 vol.% O₂ and 5 vol.% H₂O). The PdAl sample exhibited a steady and linear decrease in the CH₄ conversion during this period. This illustrates the typical loss in catalytic activity for Pd/Al₂O₃ in the presence of water vapor, caused by hydroxyl formation on the catalyst surface [6]. Interestingly, the zeolite supported samples expressed large differences in catalytic activity in the presence of water vapor, especially the beta supported samples. Both PdB511 and PdB969 exhibited very high CH₄ conversions, constantly around 91–93%, during the first 3 h of exposure to the wet reaction mixture. By contrast, the CH₄ oxidation activity for PdB40 decreased rapidly and the conversion was only 13% after 3 h. Another noteworthy observation is that PdB511 and PdB969 did not only express high but also stable activity over time, i.e. the time dependent accumulative water deactivation was almost negligible. Moreover, the similar trend was expressed by the SSZ-13 supported samples, Fig. 11. However, the difference in activity was smaller for PdS52 and PdS43, which most likely is correlated to the smaller difference in SAR for these two samples. Nevertheless, the CH₄ conversion for PdS52 decreased to around 38% after 3 h of exposure to wet reaction mixture. In comparison, the CH₄ conversion for PdS43 dropped to 11% during the same period. It should be emphasized that both PdB40, PdS52 and PdS43 showed a clear accumulative water deactivation over time, i.e. decreased activity correlated to the time on stream in the wet gas feed, whereas the stable activity for PdB511 and PdB969 indicates that the surface of highly siliceous zeolites becomes saturated with hydroxyls rather fast. Thus, already from the first 3 h of exposure to the wet gas mixture, it can be concluded that Pd supported on zeolites with high SAR has a superior tolerance to water vapor compared to zeolites with lower SAR and Al₂O₃ as a support

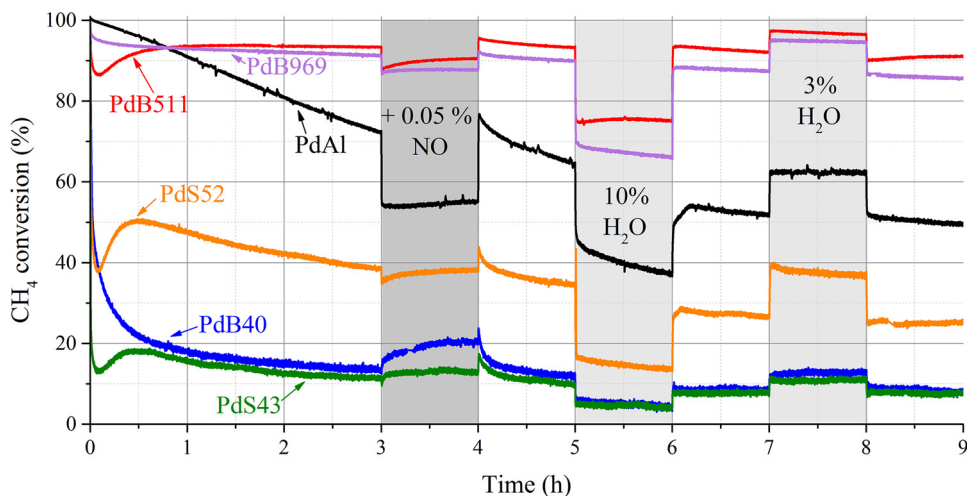


Fig. 11. Isothermal activity test with H_2O at 450°C during 9 h for PdAl (black line), PdB40 (blue line), PdB511 (red line), PdB969 (purple line), PdS43 (green line) and PdS52 (orange line). The white areas represent the wet reaction mixture (0.05 vol.% CH_4 , 8 vol.% O_2 and 5 vol.% H_2O) and the grey areas, from left to right, correspond to the addition of 0.05 vol.% NO, the change to 10 vol.% H_2O and the change to 3 vol.% H_2O , respectively. All samples were degreened and pre-treated according to the procedure in Section 2.4.1 prior to the activity test. (For interpretation of the references to colour in this figure legend, the reader is referred to the web version of this article).

material. Okumura et al. [21] associated this to the high hydrophobicity, and consequently low water adsorption, of zeolites with high SAR. However, also the zeolite structure has been reported to be crucial for the catalytic activity in the presence of water vapor. Lim et al. [19] found for instance that Pd supported on different small-pore zeolites obtained different degree of water deactivation despite similar SAR. However, here it can be seen that PdB40 and PdS43 exhibit almost identical CH_4 conversion and degree of deactivation, despite the large difference in the zeolite structure but with similar SAR. Hence, it appears that the SAR has a greater influence on the CH_4 oxidation activity in the presence of water vapor than the zeolite structure. It should also be mentioned that during the first 30 min of the experiment shown in Fig. 11, the CH_4 conversion for PdB511, PdS52 and PdS43 initially decreased and thereafter increased again. We believe that this is a combined effect of deactivating hydroxyls on the catalyst surface and the progressively increased oxidation state of the Pd upon the change from pure Ar to O_2 and water vapor containing gas feed. However, this is of minor importance for the overall interpretation of the results from this experiment.

After 3 h of exposure to the wet reaction mixture, 0.05 vol.% NO was added to the feed gas mixture (Fig. 11). It can be seen that the presence of NO strongly influenced the CH_4 oxidation activity. The addition of NO resulted in a decrease of the CH_4 conversion for PdB969, PdB511, PdAl and PdS52. On the contrary, a mild promoting effect was observed for PdB40 and almost no effect was seen for PdS43. In an earlier study [46], we examined the effect of NO and the combined effect of NO and water vapor. We suggested that the suppressed activity was caused by the formation of blocking surface compounds when NO is introduced. However, we also saw a promoting effect when NO was added in a combination with water vapor at other conditions. The suggested reason for this is the formation of HNO_2 species as NO reacts with hydroxyl groups on the surface [46]. Based on this reasoning, the high surface hydroxyl coverage attributed to the low CH_4 conversion of PdB40 may have resulted in extensive HNO_2 formation, which is a possible cause of the enhanced activity for PdB40 upon the introduction of NO. Another interesting observation in Fig. 11, is that after the removal of NO from the gas feed, the activity for all samples returned to the same level as prior to the NO introduction. Thus, the accumulative water deactivation stopped during the time when NO was present in the gas feed. This is particularly evident for the PdAl sample.

After 5 h, the interaction with water vapor was further studied by changing the water vapor concentration in the following steps: 10-5-3-5 vol.%, where each step lasted for 1 h. In Fig. 11, it can clearly be seen that the catalytic activity for all the samples rapidly decreased upon the increase in the water vapor concentration to 10 vol.%. Similarly, the CH_4 conversion was quickly enhanced for all samples when the water

vapor concentration was decreased to 3 vol.%. In a kinetic modelling study [11], we earlier proposed that the water deactivation consists of two parts; (i) water/hydroxyl adsorption on the active sites that occurs immediately when adding water and (ii) slow build-up of hydroxyl species. The changes in the CH_4 conversion correlated to the variations in water vapor concentration are caused by quick hydroxylation/dehydroxylation of the catalyst surface. This occurred for all the tested catalysts samples. However, for the highly siliceous samples, PdB511 and PdB969, the catalytic activity reversibly returned to about the same activity level as the water vapor concentration was changed back to 5 vol.%. Hence, it appears that the first route of water deactivation mentioned above, (i), is dominant, whereas the second route, (ii), is almost negligible when highly siliceous zeolite supports are used. For the other samples, both (i) and (ii) are significantly contributing to the water deactivation. In general, it can be concluded that the high SAR beta supported samples demonstrate a unique water resistance ability than the other tested samples no matter of the gas composition used in this study.

3.4. Catalytic activity in the presence of SO_2 and water vapor

The tolerance to sulfur for respective sample was tested by adding 10 ppm SO_2 to the gas feed during a period of 4 h, see Fig. 12. To clarify, Fig. 12 is the continuation of the isothermal activity test shown in Fig. 11 and the 9th hour of the experiment is displayed in both of the two figures. Although the samples showed different degrees of water deactivation prior to the SO_2 exposure, the results in Fig. 12 give a good estimation of the degree and rate of SO_2 poisoning of the samples. No clear differences in the sulfur poisoning rate can be distinguished amongst the zeolite samples. All of them rapidly lost most of their catalytic activity within the first 30 min after the introduction of SO_2 . By contrast, the PdAl sample showed a more slow and linear activity loss during the 4 h of SO_2 exposure. In order to understand the large differences in the sulfur resistance, the remaining sulfur content after SO_2 poisoning was measured with ICP-SFMS, see Table 2. Note this was made for separate monoliths of PdAl and PdB969, which had been degreened, pre-treated and thereafter poisoned with SO_2 under the same conditions (for details, see Section 2.4.4). The measured S/Pd ratio was 2.83 for PdAl and 0.25 for PdB969, hence about 10 times more sulfur was adsorbed on PdAl compared to PdB969. Lampert et al. [12] proposed that Pd/ Al_2O_3 deactivates more slowly than Pd/ SiO_2 due to the higher SO_2 adsorption on Al_2O_3 than on SiO_2 . The Al_2O_3 support was therefore thought of acting as a sulfur sink, hence preventing the formation of PdSO_x species. Hence, this finding also explains the more rapid deactivation of the zeolite samples compared to PdAl in this study. This means that the low SO_2 adsorption on the zeolite supports

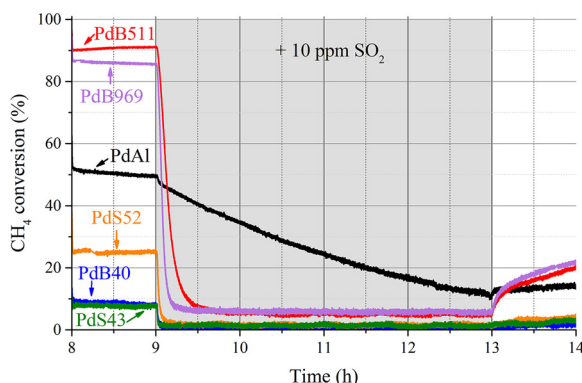


Fig. 12. Isothermal activity test with H₂O and SO₂ at 450 °C with 4 h of SO₂ poisoning for PdAl (black line), PdB40 (blue line), PdB511 (red line), PdB969 (purple line), PdS43 (green line) and PdS52 (orange line). The white areas represent the wet reaction mixture (0.05 vol.% CH₄, 8 vol.% O₂ and 5 vol.% H₂O) and the grey area corresponds to the wet reaction mixture with the addition of 10 ppm SO₂. Note that this sequence followed immediately after the isothermal activity test with H₂O (Fig. 11) without pre-treatment in between. (For interpretation of the references to colour in this figure legend, the reader is referred to the web version of this article).

Table 2

Molar ratio of sulfur to Pd content of the samples after the SO₂ poisoning and after the regeneration sequences.

	S/Pd (molar ratio)	
	After SO ₂ poisoning	After regeneration sequences
PdAl	2.83	0.25
PdB40	–	< 0.16*
PdB511	–	< 0.14*
PdB969	0.25	< 0.14*
PdS43	–	0.24
PdS52	–	0.20

* Below detection limit for ICP-SFMS.

results in the generation of more PdSO_x species and consequently a rapid activity loss. Chen et al. [38] observed that SO₂ exposure of Pd/CHA and Pd/beta resulted only in a minor decrease of the NO storage capacity. Since the NO adsorption mainly occurs on the ion-exchanged Pd²⁺ species, these Pd sites were therefore suggested to be rather insensitive to the SO₂ exposure. However, since the PdO particles appears to be most active for the CH₄ oxidation based on the dry activity test (Section 3.2), this is not likely to enhance the CH₄ oxidation which also goes in line with the results in Fig. 12. Moreover, it should be noted that the sulfur poisoning for all samples was also most likely accelerated by the presence of water, as reported previously [7,18].

Fig. 13 shows the outlet concentration of SO₂ during the poisoning sequence in Fig. 12. After about 1–1.5 h, the outlet concentration of SO₂ reached 10 ppm, i.e. the same level as the inlet concentration, for all the zeolite samples. Interestingly, the outlet concentration reached 10 ppm shortly after the point when the zeolite samples reached their minimum catalytic activity. On the contrary, no SO₂ could be detected during the sulfur poisoning of PdAl. This indicates that most of the SO₂ was adsorbed on the PdAl surface, whereas the zeolite samples reached their saturation level of SO₂ adsorption rather fast. These results agree well with the measured sulfur content of the SO₂ poisoned samples in Table 2 and support the explanation for that the zeolite supported samples are sensitive to sulfur because of the low sulfur storage capacity of the zeolite supports. However, it cannot be completely excluded that the low outlet concentration of SO₂ for the PdAl sample resulted from the formation of other gaseous sulfur compounds which could not easily be detected under experimental conditions. Moreover, by comparing Fig. 13 with the blank SO₂ profile of the reactor (empty reactor)

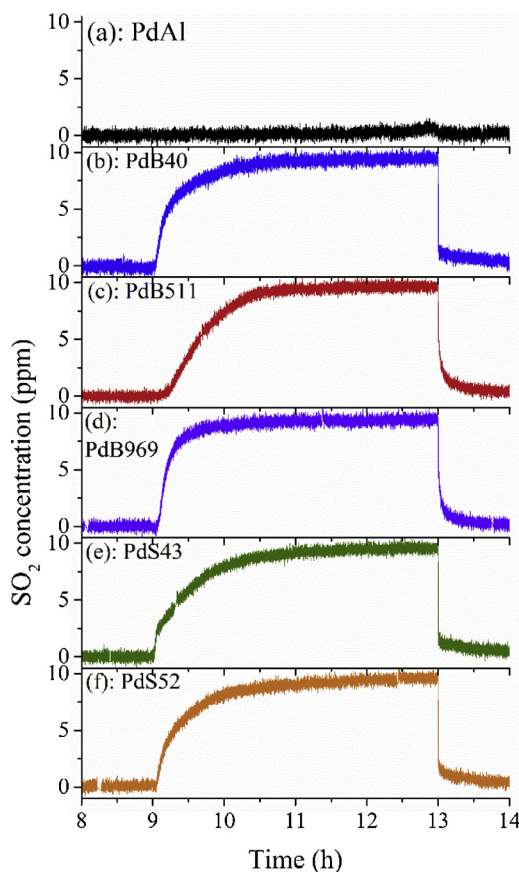


Fig. 13. Outlet concentration of SO₂ during the isothermal activity test with H₂O and SO₂ (Fig. 12) for PdAl (a, black line), PdB40 (b, blue line), PdB511 (c, red line), PdB969 (d, purple line), PdS43 (e, green line) and PdS52 (f, orange line). (For interpretation of the references to colour in this figure legend, the reader is referred to the web version of this article).

in Figure S6 (Supplementary Material), it can be seen that the reactor design had a negligible impact on the SO₂ outlet concentration profiles.

The SO₂ poisoning was followed by a sequence of four different regeneration steps which are presented in Fig. 14. Hence, Fig. 14 displays the continuation of the isothermal activity test with H₂O and SO₂ (Fig. 12) and the 14th hour of this sequence is shown in both of the figures. Between the removal of SO₂ and the first regeneration step, the reactor was fed with the wet reaction mixture for 1 h, also at 450 °C. After the removal of the SO₂ from the inlet feed, the PdAl, PdB40, PdS43 and PdS52 samples maintained about the same low level of catalytic activity as in the end of the SO₂ poisoning period. By contrast, the samples with highly siliceous beta zeolite, i.e. PdB511 and PdB969, showed an immediate slight recover as the CH₄ conversion increased from around 6% to 21% during the hour subsequent to the SO₂ poisoning step. This observation indicates that an increased SAR facilitates regeneration after SO₂ poisoning.

The first regeneration step (R1) was performed at 600 °C in the wet reaction mixture, i.e. under lean conditions and in the presence of water vapor. During R1, a large part of the catalytic activity was recovered for PdB511 and PdB969, whereas the other samples showed no or only a small degree of regeneration. However, it should also be considered that the presence of water vapor suppressed the activity, especially for PdB40, PdS43, PdS52 and PdAl. The second regeneration step (R2) was conducted at 450 °C but in rich gas mixture containing 0.05 vol.% CH₄ and 5 vol.% H₂O. Rich gas conditions has previously been reported to facilitate the sulfur regeneration [50]. Moreover, PdAl, PdS43 and PdS52 recovered most activity during R2. Indeed, the CH₄ conversion after R2 for these samples is comparable to the level just before the SO₂

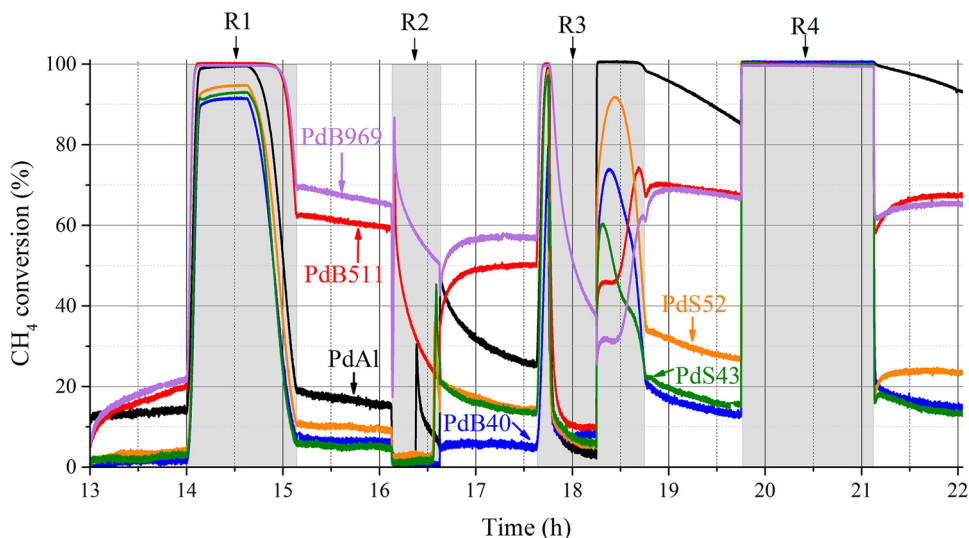


Fig. 14. Regeneration sequence consisting of 4 regeneration steps (R1- R4) subsequent to the SO₂ poisoning (Fig. 12) for PdAl (black line), PdB40 (blue line), PdB511 (red line), PdB969 (purple line), PdS43 (green line) and PdS52 (orange line). The white areas represent the wet reaction mixture (0.05 vol.% CH₄, 8 vol.% O₂ and 5 vol.% H₂O) at 450 °C and the grey areas correspond to the regeneration steps R1-R4 which are explained in Section 2.4.5. Note that this sequence followed immediately after the isothermal activity test with H₂O and SO₂ (Fig. 12) without pre-treatment in between. (For interpretation of the references to colour in this figure legend, the reader is referred to the web version of this article).

was introduced (Fig. 12). However, the activity decreased thereafter again in the wet reaction mixture, which could be an effect of either water deactivation or sulfur spillover from the support to the Pd species. This was followed by the third regeneration step (R3), which was performed by heating to 600 °C (20 °C/min) in the wet reaction mixture, followed by the removal of O₂ for 30 min, *i.e.* rich regeneration in 0.05 vol.% CH₄ and 5 vol.% H₂O for 30 min at 600 °C. Thereafter, the O₂ was reintroduced while the sample was cooled to 450 °C. Based on the subsequent 1 h of CH₄ oxidation in the wet reaction mixture, R3 did not result in any further recovery of the catalytic activity for PdB969 compared to R1. However, the catalytic activity was slightly enhanced for PdB511 after R3 compared to after R1. This may be related to the lower SAR of PdB511 in comparison to PdB969. Both PdB40, PdS43 and PdS52 obtained higher activity after R3 than prior to the SO₂ introduction (Fig. 12). This is ascribed to the combined effect of sulfur desorption and removal of surface hydroxyl groups due to the temperature increase in R3. Furthermore, the activity of PdAl was close to fully regenerated after R3 and thus PdAl obtained by far the highest degree of regeneration amongst the samples. Also here, it should be noted that this was caused by the removal of both hydroxyls and sulfur species. The forth regeneration step (R4) was conducted by heating in Ar to 600 °C, reduction in 2 vol.% H₂ and 5 vol.% water vapor for 30 min, followed by cooling to 450 °C, also in Ar. Thereafter, the wet reaction mixture was reintroduced. For all the samples, it can be seen that R4 only provided a minor contribution to the total regeneration which means that all the easily removed sulfur species were desorbed in the previous regeneration steps. The remaining sulfur content in the samples after the regeneration sequence was measured with ICP-SFMS and is displayed in Table 2. It can be seen that very little sulfur remained on the samples after these regeneration steps. However, all the beta supported samples contained less sulfur than the SSZ-13 supported samples and the PdAl. The SSZ-13 and Al₂O₃ based samples had about the same sulfur content after regeneration. This means that not only the SAR but also the zeolite structure influence the amount of sulfur remaining after regeneration.

In summary, it was found that zeolite supported Pd is highly sensitive to SO₂ and rapidly lose the majority of the catalytic activity in the presence of 10 ppm SO₂. It was also seen that a high SAR facilitates the regeneration of the catalytic activity after SO₂ poisoning, since a large part of the activity could be recovered with fewer regeneration steps compared to the equivalent samples with lower SAR. This finding also applies in comparison with the PdAl sample. Lampert et al. [12] reported that Pd/SiO₂ can be regenerated more easily than Pd/Al₂O₃. They suggested that the higher SO₂ adsorption on Al₂O₃ than on SiO₂ results in more sulfur spillover from the support to the Pd for Pd/Al₂O₃.

which impedes the recovery of the catalytic activity by the formation of new PdSO_x species. The results in Table 2 show that more SO₂ was adsorbed on PdAl than on PdB969 after the SO₂ poisoning. Therefore, we suggest that the initial rapid regeneration of PdB511 and PdB969 results from the low storage capacity of sulfur species on the siliceous zeolite supports which gives a low sulfur spillover and consequently more rapid regeneration. However, neither PdB969 nor PdB511 could be completely regenerated after SO₂ poisoning, whereas this was possible for PdAl. The remaining sulfur content after the regeneration sequence shows that PdB969 and PdB511 contained less sulfur compared to PdAl (Table 2). However, it was also seen that very small amount of adsorbed sulfur on PdB969 caused almost complete deactivation, whereas about 10 times as much adsorbed sulfur was needed to reach approximately the same level of deactivation for PdAl. Therefore, it cannot be completely excluded that remaining sulfur species on PdB969 and PdB511 caused the incomplete regeneration. Moreover, STEM images of the samples before and after the flow reactor experiments were collected in order to study the Pd sintering (Fig. 3). However, no significant degree of Pd sintering was detected. This means that Pd sintering was not the primary reason for that the siliceous beta samples could not reach full regeneration.

4. Conclusions

The influence of the SAR for beta and SSZ-13 supported Pd for complete CH₄ oxidation has been investigated with a particular focus on the effect of water vapor and SO₂. This study clearly shows that an increased SAR of the zeolite framework significantly improves the CH₄ oxidation in the presence of water vapor and results in both high and stable conversion. We suggest that this is a result of the high hydrophobicity of the highly siliceous zeolites. Furthermore, it appears that the CH₄ oxidation activity in the presences of water vapor is influenced more by the SAR than the type of zeolite framework. An increased SAR of the zeolite support was also shown to enhance the CH₄ oxidation activity under dry conditions, although the effect was larger under wet conditions. We believe that the formation of more Pd particles in relation to ion-exchanged Pd²⁺ species and changes in oxidation-reduction behavior of the Pd are responsible for the improved CH₄ oxidation activity under dry conditions. Larger Pd particles were formed on zeolites with high SAR. By contrast, zeolites with low SAR and consequently a higher number of acidic sites were able to stabilize smaller and more dispersed Pd particles in addition to a higher number of isolated Pd²⁺ species. The monoatomic Pd²⁺ species, mostly formed on the zeolites with low SAR, had significantly higher oxidation and reduction temperatures than Pd in particle form.

Moreover, zeolite supported Pd is more sensitive than Pd/Al₂O₃ to SO₂. This is addressed to the higher SO₂ adsorption on the Al₂O₃ which therefore impedes the formation of PdSO_x. In the opposite way, the low sulfur storage capacity of the zeolite supports results in the formation of more PdSO_x species. However, the catalytic activity of Pd supported on zeolites with high SAR could be regenerated easier after the SO₂ poisoning compared to Pd supported on zeolites with low SAR and Al₂O₃. The reason for this is that the low sulfur storage capacity of the highly siliceous zeolites results in less spillover of sulfur compounds from the support to the Pd. The use of supports that adsorb much SO₂, such as Al₂O₃, results in more sulfur spillover from the support to the Pd, which consequently makes the regeneration more difficult. On the other hand, Pd on siliceous zeolites could not fully regain their activity after the SO₂ poisoning, whereas this was possible for Pd/Al₂O₃.

Acknowledgements

We would like to acknowledge the financial support by the Swedish Research Council [Grant number 642-2014-5733].

Appendix A. Supplementary data

Supplementary material related to this article can be found, in the online version, at doi:<https://doi.org/10.1016/j.apcatb.2019.03.005>.

References

- [1] R. Burch, F.J. Urbano, Investigation of the active state of supported palladium catalysts in the combustion of methane, *Appl. Catal. A Gen.* 124 (1995) 121–138.
- [2] K. Fujimoto, F.H. Ribeiro, M. Avalos-Borja, E. Iglesia, Structure and reactivity of PdO/ZrO₂, catalysts for methane oxidation at low temperatures, *J. Catal.* 179 (1998) 431–442.
- [3] J. Nilsson, P.A. Carlsson, S. Fouladvand, N.M. Martin, J. Gustafson, M.A. Newton, E. Lundgren, H. Gronbeck, M. Skoglundh, Chemistry of supported palladium nanoparticles during methane oxidation, *ASC Catal.* 5 (2015) 2481–2489.
- [4] S.C. Su, J.N. Carstens, A.T. Bell, A study of the dynamics of Pd oxidation and PdO reduction by H-2 and CH₄, *J. Catal.* 176 (1998) 125–135.
- [5] M. Lyubovskiy, L. Pfefferle, Complete methane oxidation over Pd catalyst supported on alpha-alumina. Influence of temperature and oxygen pressure on the catalyst activity, *Catal. Today* 47 (1999) 29–44.
- [6] R. Gholami, M. Alyani, K.J. Smith, Deactivation of Pd catalysts by water during low temperature methane oxidation relevant to natural gas vehicle converters, *Catal.* 5 (2015) 561–594.
- [7] D.L. Mowery, R.L. McCormick, Deactivation of alumina supported and unsupported PdO methane oxidation catalyst: the effect of water on sulfate poisoning, *Appl. Catal. B Environ.* 34 (2001) 287–297.
- [8] R. Burch, F.J. Urbano, P.K. Loader, Methane combustion over palladium catalysts: the effect of carbon dioxide and water on activity, *Appl. Catal. A Gen.* 123 (1995) 173–184.
- [9] W.R. Schwartz, D. Ciuparu, L.D. Pfefferle, Combustion of methane over palladium-based catalysts: catalytic deactivation and role of the support, *J. Phys. Chem. C* 116 (2012) 8587–8593.
- [10] W.R. Schwartz, L.D. Pfefferle, Combustion of methane over palladium-based catalysts: Support interactions, *J. Phys. Chem. C* 116 (2012) 8571–8578.
- [11] N. Sadokhina, F. Ghasempour, X. Auvray, G. Smedler, U. Nyblén, M. Olofsson, L. Olsson, An Experimental and kinetic modelling study for methane oxidation over Pd-based catalyst: Inhibition by water, *Catal. Lett.* 147 (2017) 2360–2371.
- [12] J.K. Lampert, M.S. Kazi, R.J. Farrauto, Palladium catalyst performance for methane emissions abatement from lean burn natural gas vehicles, *Appl. Catal. B Environ.* 14 (1997) 211–223.
- [13] S. Ordóñez, P. Hurtado, H. Sastre, F.V. Diez, Methane catalytic combustion over Pd/Al₂O₃ in presence of sulphur dioxide: development of a deactivation model, *Appl. Catal. A Gen.* 259 (2004) 41–48.
- [14] P. Gelin, L. Urfels, M. Primet, E. Tena, Complete oxidation of methane at low temperature over Pt and Pd catalysts for the abatement of lean-burn natural gas fuelled vehicles emissions: influence of water and sulphur containing compounds, *Catal. Today* 83 (2003) 45–57.
- [15] P. Hurtado, S. Ordóñez, H. Sastre, F.V. Diez, Combustion of methane over palladium catalyst in the presence of inorganic compounds: inhibition and deactivation phenomena, *Appl. Catal. B Environ.* 47 (2004) 85–93.
- [16] L.J. Hoyos, H. Praliaud, M. Primet, Catalytic combustion of methane over palladium supported on alumina and silica in presence of hydrogen-sulfide, *Appl. Catal. A Gen.* 98 (1993) 125–138.
- [17] M. Honkanen, J.G. Wang, M. Karkkainen, M. Huuhtanen, H. Jiang, K. Kallinen, R.L. Keiski, J. Akola, M. Vippola, Regeneration of sulfur-poisoned Pd-based catalyst for natural gas oxidation, *J. Catal.* 358 (2018) 253–265.
- [18] D.L. Mowery, M.S. Grabski, T.R. Ohno, R.L. McCormick, Deactivation of PdO/Al₂O₃ oxidation catalyst in lean-burn natural gas engine exhaust: aged catalyst characterization and studies of poisoning by H₂O and SO₂, *Appl. Catal. B Environ.* 21 (1999) 157–169.
- [19] J.B. Lim, D. Jo, S.B. Hong, Palladium-exchanged small-pore zeolites with different cage systems as methane combustion catalysts, *Appl. Catal. B Environ.* 219 (2017) 155–162.
- [20] H. Maeda, Y. Kinoshita, K.R. Reddy, K. Muto, S. Komai, N. Katada, M. Niwa, Activity of palladium loaded on zeolites in the combustion of methane, *Appl. Catal. A Gen.* 163 (1997) 59–69.
- [21] K. Okumura, E. Shinohara, M. Niwa, Pd loaded on high silica beta support active for the total oxidation of diluted methane in the presence of water vapor, *Catal. Today* 117 (2006) 577–583.
- [22] A.W. Petrov, D. Ferri, F. Krumeich, M. Nachtegaal, J.A. van Bokhoven, O. Kröcher, Stable complete methane oxidation over palladium based zeolite catalysts, *Nat. Commun.* 9 (2018) 2545.
- [23] M. Haneda, T. Mizushima, N. Kakuta, Synergistic effect between Pd and non-stoichiometric cerium oxide for oxygen activation in methane oxidation, *J. Phys. Chem. B* 102 (1998) 6579–6587.
- [24] R. Burch, D.J. Crittle, B.W.L. Southward, J.A. Sullivan, The effect of SO₂ on the activity of Pd-based catalysts in methane combustion, *Catal. Lett.* 72 (2001) 153–155.
- [25] Z.K. Zhang, L.Y. Xu, Z.L. Wang, Y.J. Xu, Y.F. Chen, Pd/H beta-zeolite catalysts for catalytic combustion of toluene: Effect of SiO₂/Al₂O₃ ratio, *J. Nat. Gas Chem.* 19 (2010) 417–421.
- [26] J.S. McEwen, T. Anggara, W.F. Schneider, V.F. Kispersky, J.T. Miller, W.N. Delgass, F.H. Ribeiro, Integrated operando X-ray absorption and DFT characterization of Cu-SSZ-13 exchange sites during the selective catalytic reduction of NO_x with NH₃, *Catal. Today* 184 (2012) 129–144.
- [27] L. Olsson, K. Wijayanti, K. Leistner, A. Kumar, S.Y. Joshi, K. Kamasamudram, N.W. Currier, A. Yezzerat, A multi-site kinetic model for NH₃-SCR over Cu/SSZ-13, *Appl. Catal. B: Environ.* 174 (2015) 212–224.
- [28] M. Muller, G. Harvey, R. Prins, Comparison of the dealumination of zeolites beta, mordenite, ZSM-5 and ferrierite by thermal treatment, leaching with oxalic acid and treatment with SiCl₄ by H-1, Si-29 and Al-27 MAS NMR, *Microporous Mesoporous Mater.* 34 (2000) 135–147.
- [29] M. Bjørgen, S. Kolboe, The conversion of methanol to hydrocarbons over dealuminated zeolite H-beta, *Appl. Catal. A Gen.* 225 (2002) 285–290.
- [30] M.R. Apelian, A.S. Fung, G.J. Kennedy, T.F. Degnan, Dealumination of zeolite beta via dicarboxylic acid treatment, *J. Phys. Chem.* 100 (1996) 16577–16583.
- [31] J. Lee, Y. Ryoo, S.J. Cho, H. Lee, C.H. Kim, D.H. Kim, Investigation of the active sites and optimum Pd/Al of Pd/ZSM-5 passive NO adsorbers for the cold-start application: Evidence of isolated-Pd species obtained after a high-temperature thermal treatment, *Appl. Catal. B: Environ.* 226 (2018) 71–82.
- [32] M. Ogura, M. Hayashi, S. Kage, M. Matsukata, E. Kikuchi, Determination of active palladium species in ZSM-5 zeolite for selective reduction of nitric oxide with methane, *Appl. Catal. B: Environ.* 23 (1999) 247–257.
- [33] Y. Zheng, L. Kovarik, M.H. Engelhard, Y. Wang, Y. Wang, F. Gao, J. Szanyi, Low-Temperature Pd/Zeolite Passive NO_x Adsorbers: Structure, Performance, and Adsorption Chemistry, *J. Phys. Chem. C* 121 (2017) 15793–15803.
- [34] B.J. Adelman, W.M.H. Sachtler, The effect of zeolitic protons on NO_x reduction over Pd/ZSM-5 catalysts, *Appl. Catal. B: Environ.* 14 (1997) 1–11.
- [35] K. Okumura, M. Niwa, Regulation of the dispersion of PdO through the interaction with acid sites of zeolite studied by extended X-ray absorption fine structure, *J. Phys. Chem. B* 104 (2000) 9670–9675.
- [36] Y. Ryoo, J. Lee, S.J. Cho, H. Lee, C.H. Kim, D.H. Kim, Activation of Pd/SSZ-13 catalyst by hydrothermal aging treatment in passive NO adsorption performance at low temperature for cold start application, *Appl. Catal. B: Environ.* 212 (2017) 140–149.
- [37] K. Chakarova, E. Ivanova, K. Hadjiivanov, D. Klissurski, H. Knozinger, Co-ordination chemistry of palladium cations in Pd-H-ZSM-5 as revealed by FTIR spectra of adsorbed and co-adsorbed probe molecules (CO and NO), *Phys. Chem. Chem. Phys.* 6 (2004) 3702–3709.
- [38] H.Y. Chen, J.E. Collier, D.X. Liu, L. Mantarosie, D. Duran-Martin, V. Novak, R.R. Rajaram, D. Thompsell, Low Temperature NO Storage of Zeolite Supported Pd for Low Temperature Diesel Engine Emission Control, *Catal. Lett.* 146 (2016) 1706–1711.
- [39] F. Lonyi, H.E. Solt, J. Valyon, H. Decolatti, L.B. Gutierrez, E. Miro, An operando DRIFTS study of the active sites and the active intermediates of the NO-SCR reaction by methane over In,H- and In,Pd,H-zeolite catalysts, *Appl. Catal. B Environ.* 100 (2010) 133–142.
- [40] B. Pommier, P. Gelin, On the nature of Pd species formed upon exchange of H-ZSM5 with Pd(NH₃)₄(2+) and calcination in O₂, *Phys. Chem. Chem. Phys.* 1 (1999) 1665–1672.
- [41] J.M. Watson, U.S. Ozkan, Adsorption characteristics of sol-gel Gd-Pd/TiO₂ catalysts in reduction of nitric oxide with CH₄: DRIFTS and TPD, *J. Catal.* 210 (2002) 295–312.
- [42] J.A. Loiland, R.F. Lobo, Oxidation of zeolite acid sites in NO/O₂ mixtures and the catalytic properties of the new site in NO oxidation, *J. Catal.* 325 (2015) 68–78.
- [43] K. Hadjiivanov, J. Saussey, J.L. Freysz, J.C. Lavallee, FT-IR study of NO + O₂ co-adsorption on H-ZSM-5: re-assignment of the 2133 cm⁻¹ band to NO+ species, *Catal. Lett.* 52 (1998) 103–108.
- [44] H.Y. Chen, Z.H. Wei, M. Kollar, F. Gao, Y.L. Wang, J. Szanyi, C.H.F. Peden, NO oxidation on zeolite supported Cu catalysts: formation and reactivity of surface nitrates, *Catal. Today* 267 (2016) 17–27.
- [45] M. Ahrens, O. Marie, P. Bazin, M. Daturi, Fe-H-BEA and Fe-H-ZSM-5 for NO₂ removal from ambient air - A detailed in situ and operando FTIR study revealing an

- unexpected positive water-effect, *J. Catal.* 271 (2010) 1–11.
- [46] N. Sadokhina, G. Smedler, U. Nylin, M. Olofsson, L. Olsson, The influence of gas composition on Pd-based catalyst activity in methane oxidation - inhibition and promotion by NO, *Appl. Catal. B Environ.* 200 (2017) 351–360.
- [47] O. Mihai, G. Smedler, U. Nylin, M. Olofsson, L. Olsson, The effect of water on methane oxidation over Pd/Al₂O₃ under lean, stoichiometric and rich conditions, *Catal. Sci. Technol.* 7 (2017) 3084–3096.
- [48] I. Friberg, N. Sadokhina, L. Olsson, Complete methane oxidation over Ba modified Pd/Al₂O₃: The effect of water vapor, *Appl. Catal. B Environ.* 231 (2018) 242–250.
- [49] R. Roldan, A.M. Beale, M. Sanchez-Sanchez, F.J. Romero-Salguero, C. Jimenez-Sanchidrian, J.P. Gomez, G. Sankar, Effect of the impregnation order on the nature of metal particles of bi-functional Pt/Pd-supported zeolite Beta materials and on their catalytic activity for the hydroisomerization of alkanes, *J. Catal.* 254 (2008) 12–26.
- [50] F. Arosio, S. Colussi, G. Groppi, A. Trovarelli, Regeneration of S-poisoned Pd/Al₂O₃ catalysts for the combustion of methane, *Catal. Today* 117 (2006) 569–576.